Metallurgical Impact of Switching from Hammer Units to Hydraulic Presses for Forging

A Senior Project

Presented to

the Faculty of the Materials Engineering Department

California Polytechnic State University - San Luis Obispo

By

Cole Hawker

Jacob Reed

June 2024

Table Of Contents

Abstract

Carlton Forge Works (CFW) is evaluating the retirement of its hammer units in favor of hydraulic presses to address safety concerns in forging aerospace components. This paper investigates the metallurgical implications of this transition, emphasizing the importance of superior microstructures and meeting industry standards and customer requirements. The alloys in question are Titanium-6Al-4V (Ti64) and Inconel 718 (INCO 718), which comprise a majority of CFW's production. Ti64's high specific strength and thermal stability make it ideal for aerospace applications, while INCO 718 is recognized for superior high-temperature creep performance. Defects like freckles and white spots in INCO 718 are analyzed for their impact on mechanical properties. The influence of forging techniques on alloy microstructures is examined, particularly in Ti64's dynamic globularization and flow instabilities and INCO 718's grain size variations. The findings contribute valuable insights to aid CFW in the decision-making process, ensuring safety, efficiency, and quality in their forging processes.

1. Introduction

1.1 Carlton Forge Works

Carlton Forge Works (CFW) produces seamless rolled rings primarily for the aerospace industry. The significance of forging components with superior microstructures and mechanical properties cannot be overstated, especially given the critical roles these parts play within this high-stakes sector. Achieving optimal performance and reliability is paramount in meeting the stringent standards and demands of the industries in which they are a crucial supplier of parts.

1.2 Problem Statement

CFW (the sponsor of this project) is considering retiring its hammer units, and moving forging work that is currently being carried out on its hammer units to hydraulic presses. However, the project sponsor would like to understand the metallurgical impact of switching from hammer units to hydraulic presses before it makes a decision regarding retiring its hammer units. This change is brought about due to safety concerns regarding its hammer forging process. Workers must pull hot billets out of the furnace using tongs and transfer them to the hammer. Once at the hammer, one worker must control the lever which releases the hammer, while another manipulates the workpiece in close proximity. With the hammer forge, there is a greater chance of catastrophic failure of the workpiece resulting in an explosion of hot metal at high velocities, jeopardizing the safety of the workers involved. It is anticipated that this shift to hydraulic press forging would enhance safety and contribute to a safer and more efficient manufacturing environment.

2. Background

2.1 Significance of Forging

Forging is defined as the method by which the shaping of a workpiece is achieved in the solid state through the application of compressive forces using dies and tools [1]. This process, rooted in ancient history, remains a fundamental technique for transforming raw materials into intricate and functional components. Forging can be executed through two primary methods: hammering and pressing. Both involve the application of force to mold metal into the desired shape.

The historical significance of forging dates back thousands of years, making it one of the oldest known metalworking processes in human civilization. The art of forging can be traced to as early as 4,500 BCE, evident in the settlements of Mesopotamia. In this ancient era, forging played a pivotal role in the survival of communities, as people forged copper to craft essential hand tools and weapons [2] [3]. The early roots of forging emphasize its crucial role in shaping the technological evolution of human societies. The enduring nature of forging as a metalworking technique highlights its adaptability and effectiveness across historical and cultural contexts. From the railroads that powered American westward expansion, to the sophisticated components of the modern automotive and aerospace industry, the principles of forging have endured and evolved, showcasing its continued relevance and importance in human technological advancement.

2.2 Hammer Forging

The most common type of forging equipment is the hammer and anvil (Figure 1). This process is characterized by multiple impact blows on the workpiece between contoured dies. The hammer can be powered by various means such as steam, air, gravity, or hydraulics, to deform and shape a workpiece into a desired form. This process is widely used in the production of high-strength components and offers advantages in terms of precision, control, and the ability to achieve complex geometries [4].

The hammer forging process is applicable to a wide range of metal alloys such as steel, aluminum, titanium, and nickel. The process typically begins with the preparation of a billet, which is a preformed piece of material. In the production of seamless rolled rings, this billet is almost always a cylindrical shape in the size required to produce the desired final component. Before the forging process begins the billet is heated to an optimal forging temperature to improve its malleability, reduce deformation resistance, and facilitate plastic deformation during forging. The pre-heating of the billet is

crucial for achieving the required forging temperature, which is influenced by factors such as material composition, desired microstructure, and the complexity of the component [5]. Hammer forging generally introduces strain rates between 10-100 /sec [6]. Due to the high energy impacts on the billet during hammer forging, there is a likelihood of localized heating, which can alter the final microstructure of the final part.

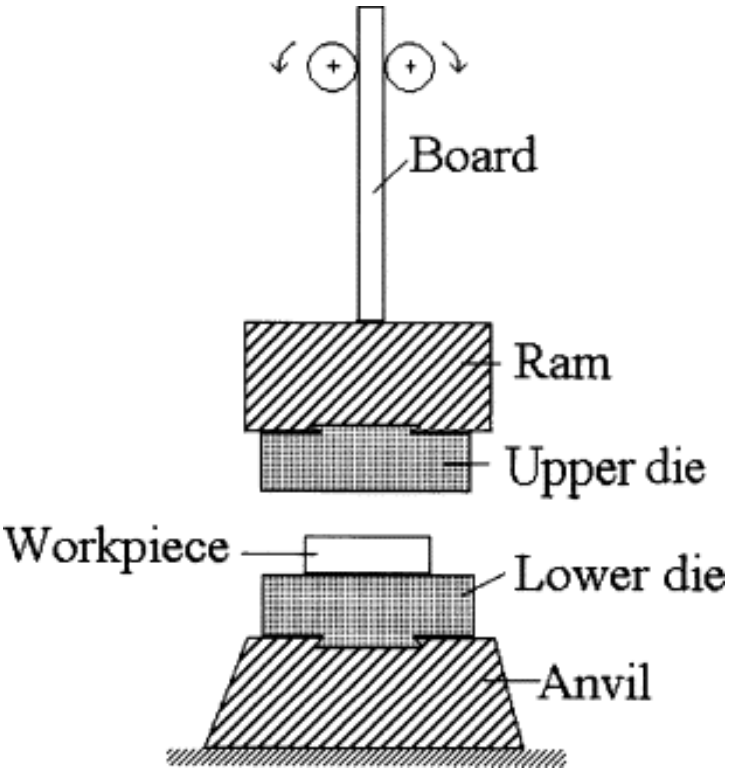

Figure 1. Schematic showing the principal components of a gravity-drop hammer forge [7].

2.3 Hydraulic Press Forging

The operation of hydraulic presses relies on hydraulic or fluid pressure, utilizing a piston to generate the required deformation load (Figure 2). The deformation load is determined by the product of fluid pressure and the cross-sectional area of the piston head. Various fluids, including water, certain emulsions, or mineral oil, serve as working fluids in the hydraulic press. Press forging subjects the material to a slow-speed compressive force causing material to flow. Unlike the impulse blows in hammer forging, press forging involves continuous, uniform pressure applied to the workpiece. Press forging is generally used for large and heavy components. The controlled and sustained nature of the force enables precise shaping and deformation [5].

Some notable distinctions between press and hammer forging lie in the handling of the pre-heated billets, material flow, and strain rates on the material. Subjecting the billet to a continuous force minimizes the likelihood of localized heating, providing greater control of the temperature throughout the forging process. The slow nature of press forging introduces strain rates significantly lower than hammer forging, ranging from 0.01 - 0.1 / sec [5]. Also, due to the sustained and slow squeeze force of press forging, there is greater control over the material flow, allowing for easier processing of precise parts in comparison to hammer forging [8].

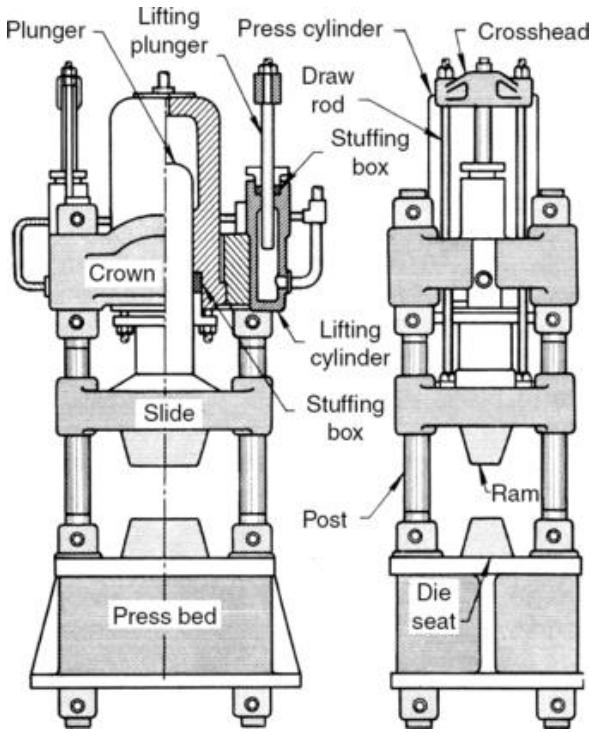

Figure 2. Schematic showing the principal components of a four-post hydraulic press [8].

2.4 Open and Closed Die Forging

Forging operations on both the hammer and press can be classified in two ways: open die forging and closed die forging. In open die forging, the load makes contact with the billet between two flat dies (Figure 3), allowing the material to flow and spread laterally. The lack of confinement in open die forging provides flexibility in shaping very large and complex components. This process is extremely reliant on skilled operators who adjust the tooling and manipulate the workpiece to achieve the desired geometry [9][10]. Closed die forging, also known as impression, die forging, involves the use of dies that contain a cavity matching the final shape of the part (Figure 4). The heated billet is placed between the dies, and the

hammer delivers precise blows that force the material to fill the cavity, resulting in a near-net shape. This method offers higher precision and better material utilization compared to open die forging [11].

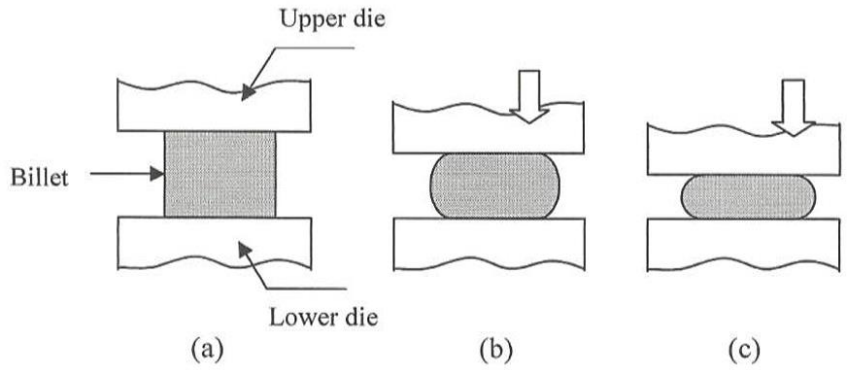

Figure 3. Illustration of open die forging [9].

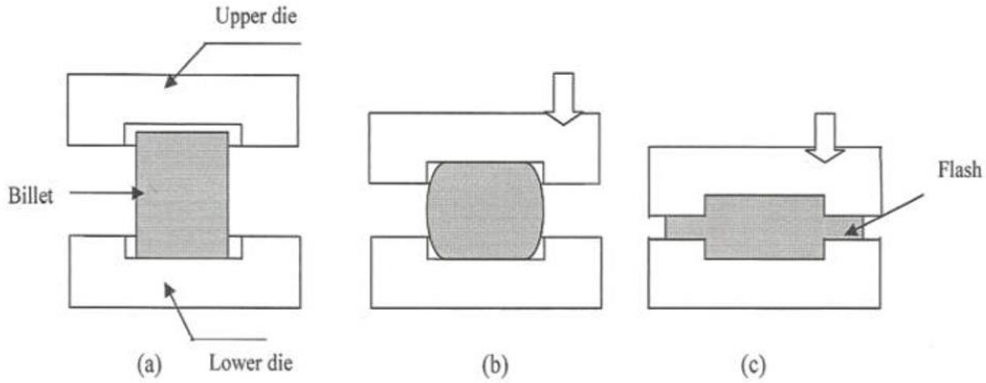

Figure 4. Illustration of closed die forging [11].

The choice between using open die forging or closed die forging depends on factors such as the complexity of the part, desired tolerances, and the required material flow. Open die forging, with its greater freedom of material movement, is suited for components where deformation needs to be controlled and localized. However, open die forging relies on a skilled operator and produces forgings with lesser accuracy [12]. Closed die forging, with its defined cavity, provides higher precision, making it ideal for intricate parts requiring tight tolerances [10].

3. Forging Alloys

An understanding of forging processes sets the stage for exploring the specific requirements and challenges associated with forging aerospace components. As we delve into the next section, we transition from the general discussion of forging techniques to focus on titanium and nickel-base alloys. These alloys make up roughly 90% of CFW's production. The unique characteristics of these alloys will be discussed, along with common defects that are crucial to mitigate in aerospace applications.

3.1 Titanium

Many of titanium's properties make it a popular choice for use in aerospace applications. Primarily, the high specific strength (defined as strength divided by density) of titanium makes it an obvious choice for aircraft, where reducing weight is of high importance [13]. An industry example of this is the Boeing 777x, where the switch from steel to titanium landing gear reduced total weight by 600 pounds for the main landing gear [13]. Secondarily, and more important for the aircraft's engines, are the thermal properties of titanium. When compared with steel, the coefficient of thermal expansion (CTE) of titanium is approximately 75% lower [14]. Not only does this preserve dimensional stability (which is important for high bypass aircraft engines), but it also improves the compatibility of titanium with other materials; Polymer matrix composites (PMC's) typically have a CTE closer to that of titanium than steel, for example. Finally, the corrosion properties of titanium are highly desirable in the aerospace industry [15]. This is primarily due to the passive nature of the thick oxide layer common in titanium alloys.

3.1.1 Titanium-6Al-4V

Titanium-6Al-4V (hereafter referred to as "Ti64") is an alloy originating in the 1950s with its first uses primarily in military applications. It is composed of 90 wt% titanium, 6 wt% aluminum, and 4 wt% vanadium. Aluminum acts as an alpha phase stabilizer in the titanium, while vanadium acts as a beta phase stabilizer in the titanium [16]. The resulting Ti64 is an alpha-beta titanium alloy; it has both alpha and beta phases in its crystal structure. It has since been used extensively in aerospace applications for its high strength-to-weight properties and corrosion resistance [17].

3.2 Nickel-based Superalloys

Originally known as high temperature alloys, superalloys are most commonly used in applications where the part is exposed to high temperatures and stress for prolonged periods of time. Such a situation often leads to failure, or dimensional changes brought about by creep. These alloys are

specifically designed to have excellent high temperature qualities; this typically means high creep resistance, high temperature corrosion resistance, and maintaining mechanical properties under high temperature. For example, nickel-based superalloys such as Inconel 718 outperform high chromium creep-resistant steels at similar temperatures [18] [19].

3.2.1 Inconel 718

Inconel 718 is a common industry superalloy best known for its ability to keep its mechanical properties at elevated temperatures, corrosion resistance, and weldability [20]. The composition of Inconel 718 (hereafter referred to as INCO 718) is 50 wt% nickel, 17-21 wt% chromium, 17 wt% iron, 5 wt% niobium, and 3 wt% molybdenum, with other minor alloying metals such as titanium and aluminum. [21]. The main phases found within INCO 718 are the γ, γ', γ'', Laves, and various carbides and nitrides (Figure 5). The γ phase makes up the majority of the material, and the γ' and γ'' phases are thought to be the primary contributors to the strength of the material. The Laves phase contains more niobium and leaves the surrounding region depleted of niobium [22]. The Laves phase is also associated with defects (most commonly brittle fracture of the phase) and generally lowers mechanical performance [22].

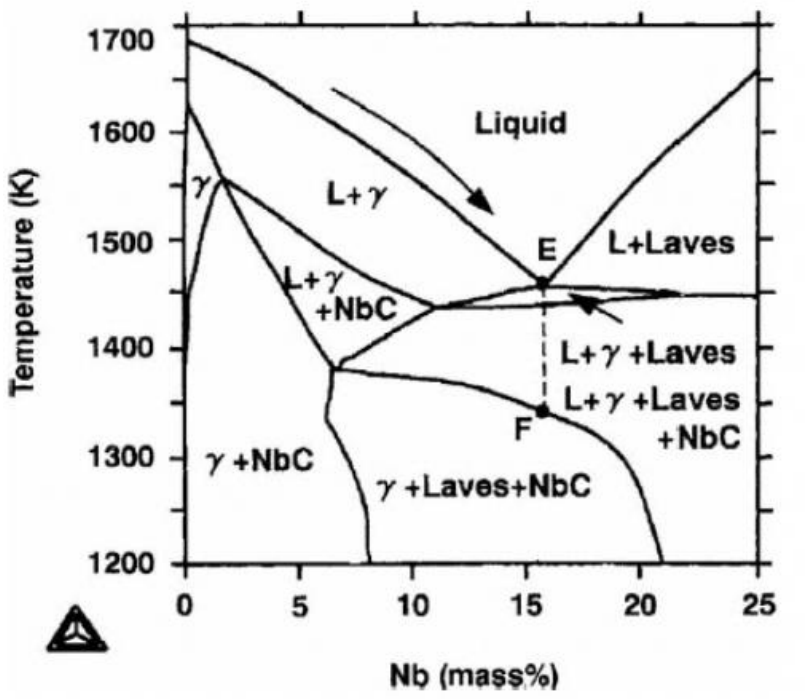

Figure 5. INCO 718 Niobium phase diagram, assuming nominal amounts of other constituent elements [23].

3.2.1.1 Freckles in INCO 718

It should first be noted that freckles are an extremely rare defect; however, they represent a serious enough issue to mandate a pause in manufacturing when they are discovered. Therefore, investigation into why freckles in nickel-based superalloys are so detrimental to the material properties is needed. Freckles themselves are areas containing a high amount of niobium similar in chemistry to the γ' phase and are associated with areas of segregation (Figure 6) [24]. Freckles are commonly caused by an abundance of the Laves phase within the region, and typically leave a niobium-depleted region behind.

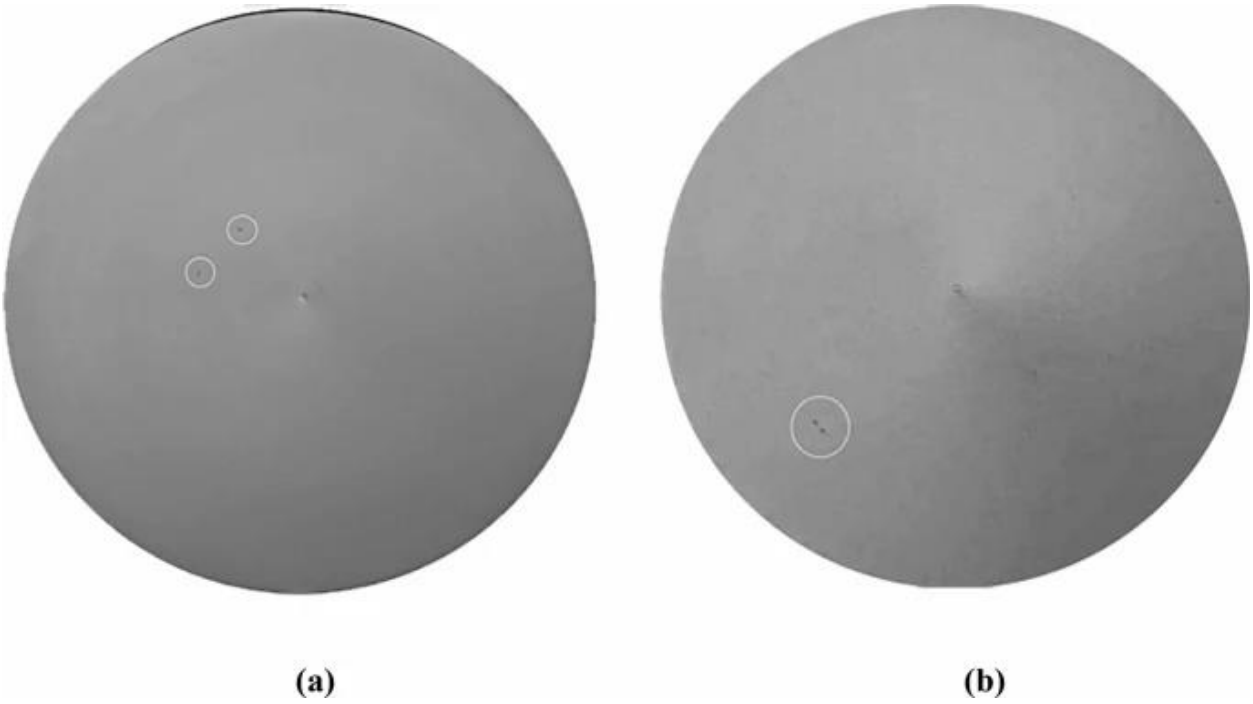

Figure 6. (a) Segregation spots and (b) freckle in 80 mm diameter billet [24].

The mechanical properties of the region surrounding the freckle are also highly impacted. It should be noted that Laves phase segregation alone does not cause any noticeable difference in tensile strength, but the presence of freckles makes a significantly negative impact on the ductility and tensile strength of the material [24]. The fatigue life of the material is also negatively affected. The Laves phase associated with freckles is thought to act as a crack initiation point in fatigue failure and therefore reduces the low cycle fatigue capability of the alloy [22].

3.2.1.2 White Spots in INCO 718

White spots are regions in INCO 718 that are depleted of niobium, titanium, and aluminum. The white spots can come in multiple forms: dendritic, discrete, and solidification [26]. Niobium is important in the strength of the INCO 718 alloy due to its contribution to solid solution strengthening and its formation of γ' and γ'' phases. Dendritic white spots are characterized by a branched or tree-like structure and indicate areas where the solidification process may have been non-uniform. Discrete white spots, appearing as distinct regions with altered composition, suggest localized temperature variation during alloy forming or subsequent processing. The reduced amount of niobium in these white spots is directly correlated with a decrease in the mechanical performance of the material [24]. Addressing and preventing the formation of these white spots is crucial for maintaining the mechanical integrity of the INCO 718 alloy.

4. Influence of Forging on Alloy Microstructure

Changes in heating during the deformation process can have a major effect on the plastic flow and microstructure evolution during forging. This effect is especially prevalent for two-phase aerospace materials such as titanium-based alloys and nickel-based superalloys. The high-temperature phase (bcc β in Ti64 and fcc γ phase in INCO 718) are much softer than their low-temperature phase (hcp α in Ti64 and fcc γ' in INCO 718). As a result, temperature changes during the metal working process can lead to non-uniform plastic flow and therefore inhomogeneous microstructure evolution [27] [28].

4.1 Influence of Forging on the Microstructure of Ti-64

Dynamic globularization and flow instabilities are common mechanisms that influence microstructural changes in Ti64. These changes are controlled by two forging parameters: temperature and strain rate [29].

4.1.1 Dynamic Globularism

Dynamic globularism is a microstructure transformation process that occurs during hot deformation. It involves the transformation of elongated, lamellar α grains into more equiaxed, globular grains. This transformation is most favorable at temperatures between 850ºC and 950ºC, with lower strain rates promoting globularization (Figure 7) [30]. Dynamic globularism can improve ductility and toughness and reduce the tendency to crack during the forging process. Globular grains have a lower aspect ratio than lamellar grains and are therefore less susceptible to stress concentrations. With lower

strain rates being associated with press forging, it is expected that press forging would better promote dynamic globularization in Ti64 parts [31].

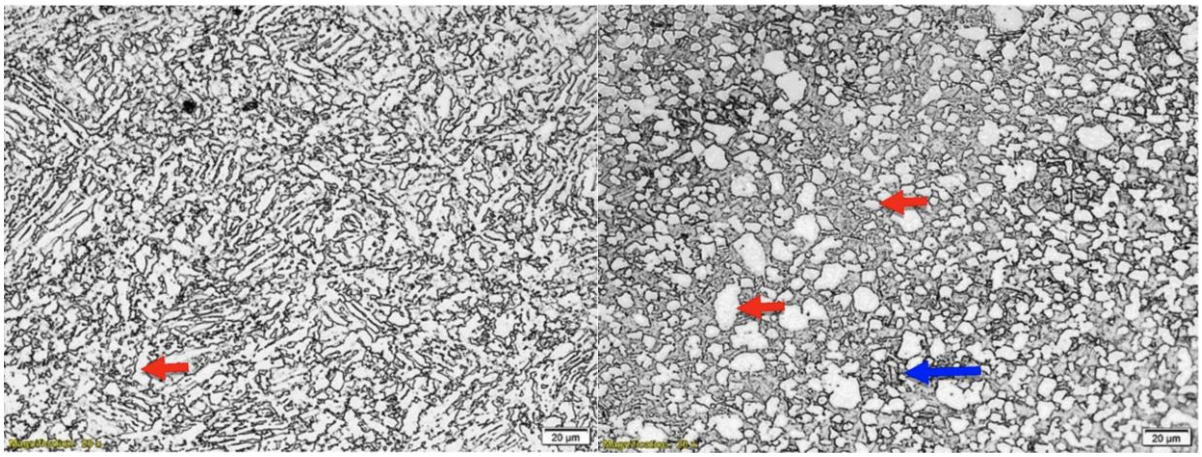

Figure 7. Optical micrograph of Ti64 deformed at a strain rate of 0.01 s^{-1}. (Left) 800 ℃, lamellar structure with red arrow indicating α-phase. (Right) 900 ℃, globular structure with red arrow indicating lighter α-phase, blue arrow indicating darker β-phase [30].

4.1.2 Flow Instability

Flow instabilities are localized shear bands that form in Ti64 during the forging process. They can lead to a number of defects including surface cracking, internal stress ruptures, and reduced ductility. The occurrence of these shear bands is found to decrease with increasing temperature and decreased strain rate (Figure 8) [32][27]. With press forging introducing lower strain rates than hammer forging, it would be expected that flow instabilities would be better mitigated with the use of a press.

4.2 Influence of Forging on the Microstructure of INCO 718

An optimal microstructure in INCO 718 is essential for providing the required material properties. Within this context, forging is a crucial step that significantly shapes the grain size and distribution, as well as influencing features like white spots. This section explores the technical nuances of how forging parameters affect the grain structure and defects in INCO 718, offering an understanding of the alloy's behavior under different temperature and strain rate conditions.

4.2.1 Grain Size

As seen with other forms of hot processing, the temperature during forging is found to be critical to the grain size and shape of the final microstructure. Working INCO 718 at a strain rate of 0.1 s^{-1} at 975°C results in fine, elongated grains. At the same strain rate, progressively higher grain diameter and a

more equiaxed grain shape are observed at 1000°C and 1050°C (Figure 9) [33]. It should be noted that some concerns arise at temperatures above 1050°C; if allowed to age at these temperatures, INCO 718 can have a dramatic reduction in yield strength [34]. This can be alleviated, however, with proper heat treatment to allow for precipitation hardening.

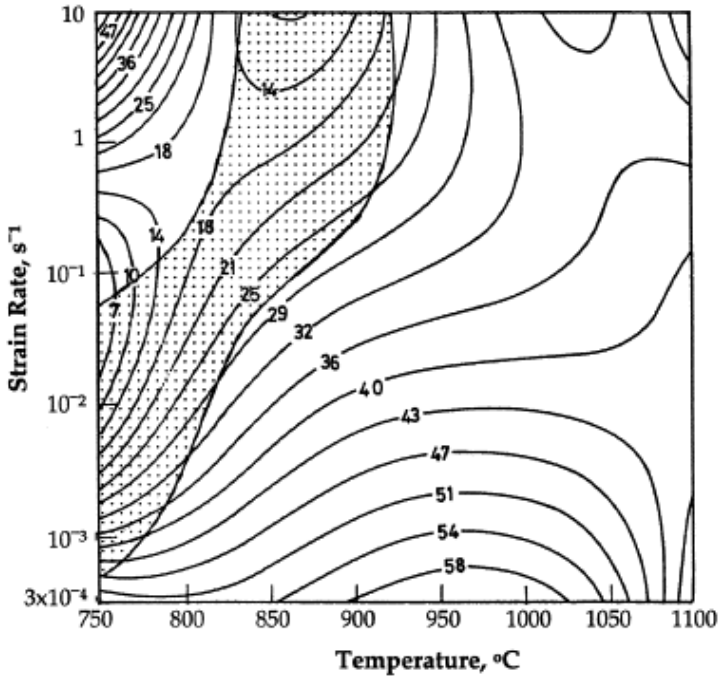

Figure 8. Contour map for forging of Ti64. The shaded region represents flow instability from a range of 825℃ to 925℃ at high strain rates [27].

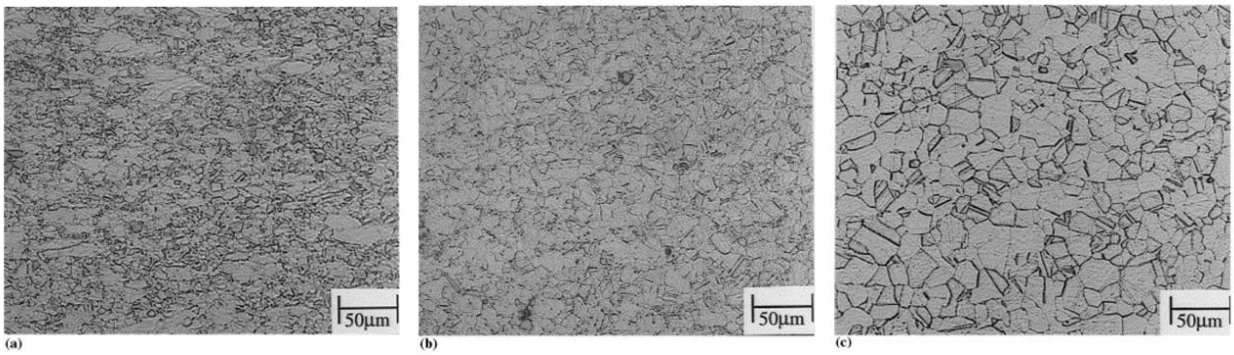

Figure 9. (a) Grain structure comparison of INCO 718 forged at 0.1 s^{-1} strain rate at 975°C, (b) 1000°C, and (c) 1050°C [33].

The strain rate of the forging method also plays a role in the microstructure of the final material. Higher strain rates typically lead to finer grains with more uniform grain size, whereas the lower strain rates associated with the hydraulic presses at CFW lead to larger grains with a greater size distribution.

This implies some potential to change the microstructure of the material if the heat treatment used does not properly recrystallize the grains [33].

Grain structure has a stronger dependence on temperature than strain rate. Nevertheless, using different strain rates can produce a visible difference in grain structure. Figure 10 shows how using a higher strain rate in forging can result in a finer grain structure.

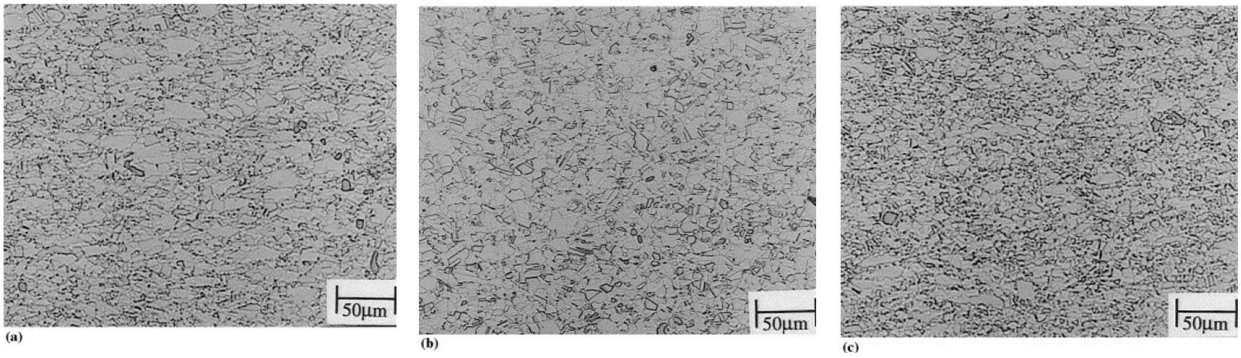

Figure 10. Grain structure comparison of INCO 718 forged at 975°C and a strain rate of (a) 0.01 s^{-1}, (b) 0.1 s^{-1}, and (c) 1 s^{-1} [33].

The microstructure caused by strain rates associated with hammer forging (10 – 100 s^{-1}) can be significantly different from that produced by the slower strain rates of hydraulic presses. Figure 11 shows the grain structures of INCO 718 hammer forged at similar temperatures as the INCO 718 shown in Figures 9 and 10. Under hammer forging, INCO 718 has been shown to have more niobium and titanium carbides and less uniform grain sizes [34].

4.2.2 White Spots

There is little research on the effects of hammer or hydraulic press forging on the frequency and severity of white spots. However, many studies have investigated the effects of (vacuum arc remelted) VAR ingots. VAR is a process in which ingots of the superalloy are remelted under vacuum using an arc as the heat source. This process helps the alloys meet the strict standards of aerospace applications; after this process, the alloy typically has a more uniform grain structure and is closer to nominal metal ratios for the alloy [35]. This process strongly affects the type and frequency of white spots present in the alloy. Specifically, the solidification rate (and therefore temperature of the arc) is important. It has been observed that sudden changes in solidification rate can result in the formation of white spots [36]. However, thorough remelting processes can alleviate this issue and produce ingots virtually free of white spots. Melting raw materials using traditional arc furnaces, decarburizing, and conducting two separate

VAR processes in series can eliminate white spots or freckles [37]. Overall, it is unknown how forging techniques affect the white spot formation in superalloys, but it is clear from the literature that the VAR process commonly used on these superalloys affects the presence of white spots.

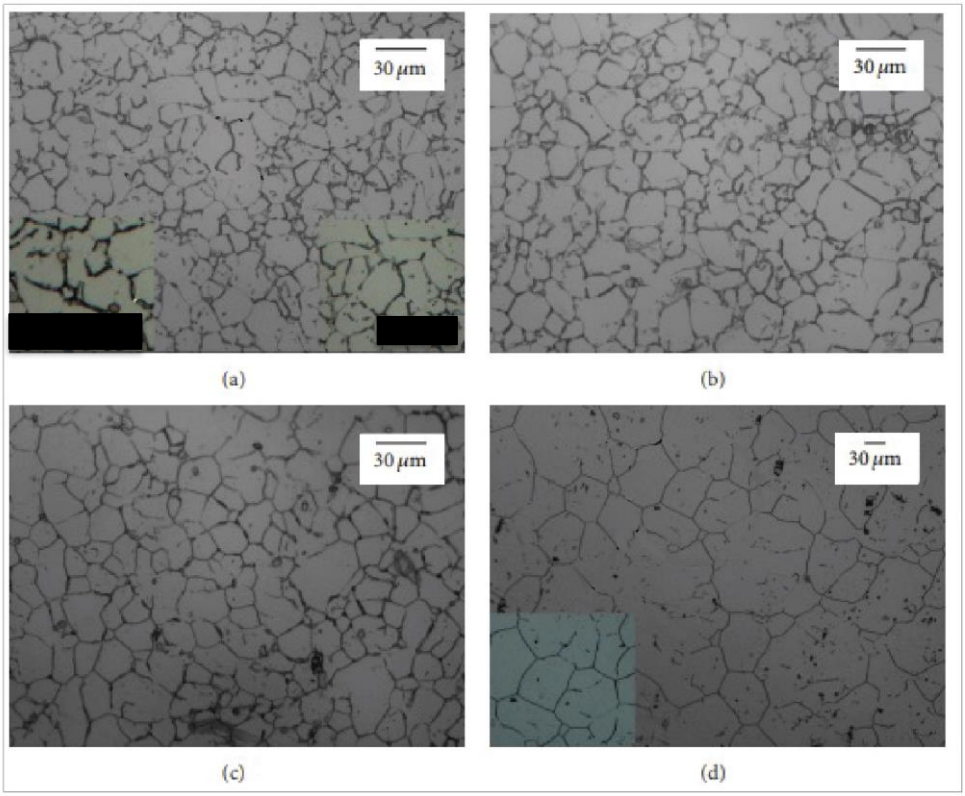

Figure 11. Grain structure comparison of hammer forged INCO 718 at temperatures of (a) 900°C, (b) 940°C, (c) 980°C, and (d) 1050° [34].

5. Research Question

What are the metallographic (grain size, phase distribution, grain structure, defects) differences in Ti64 and INCO 718 when comparing hydraulic press and hammer forging of seamless rolled rings?

6. Methodology

6.1 Samples

After consulting with the Cal Poly statistics consultant and CFW, it was decided that eight samples from each type of forging (hammer and hydraulic press) would be sufficient in determining if any metallographic differences in the samples exist due to the forging method. One billet was created

from Ti64 using each forging method, resulting in billets 47 and 48. The same was done with INCO 718, resulting in billets 43 and 44. To reduce bias, single blind testing conditions were used where the Cal Poly project participants were not told by CFW which of these was created using the hammer forge and which was created using hydraulic press forging until after data collection and data analysis were completed. For both alloys, one billet from each forging method was cut into quarters axially, and samples were collected from two of these quarters. These two quarters were opposite each other and did not share a flat face (Figure 12).

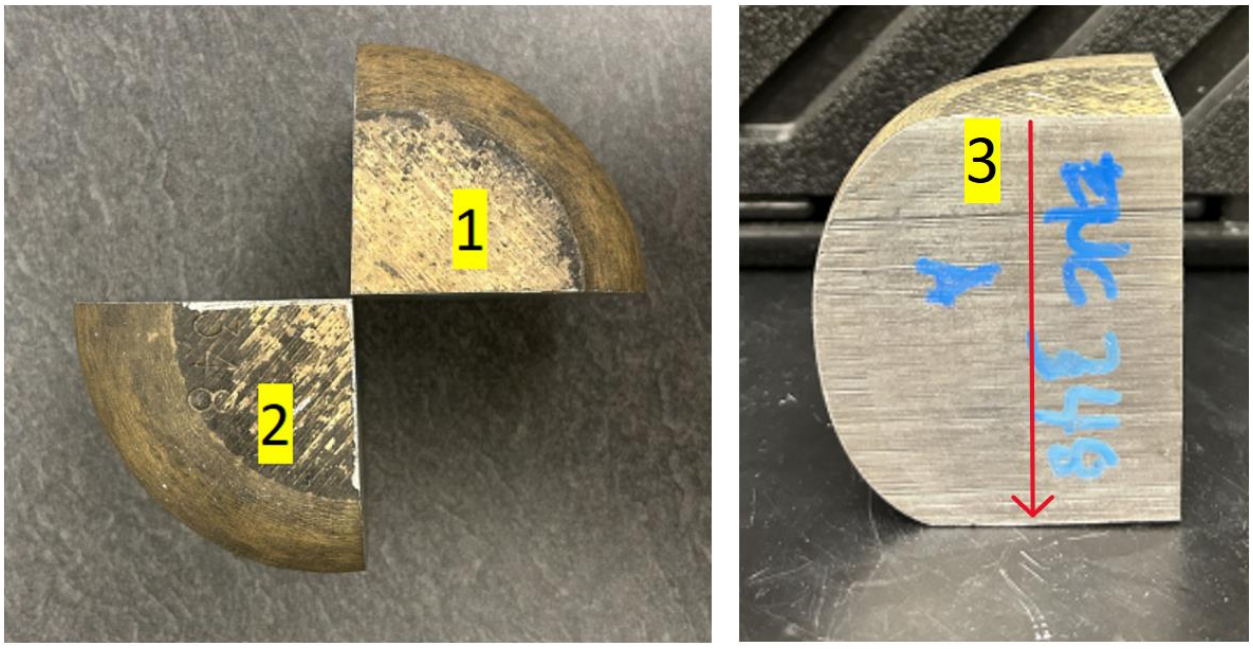

Figure 12. Ti-64 quarters cut from billet: 1) Quarter 47-C, 2) Quarter 47-A, and 3) Direction of force from hammer or hydraulic press platen (axial direction).

Within each of the two quarters, two samples were from the top of the billet, one sample from the middle of the billet, and one sample from the bottom of the billet. “Top” in this case refers to the surface of the sample closest to the hammer face or hydraulic press platen, whereas “bottom” refers to the sample surface closest to the ground during forging.

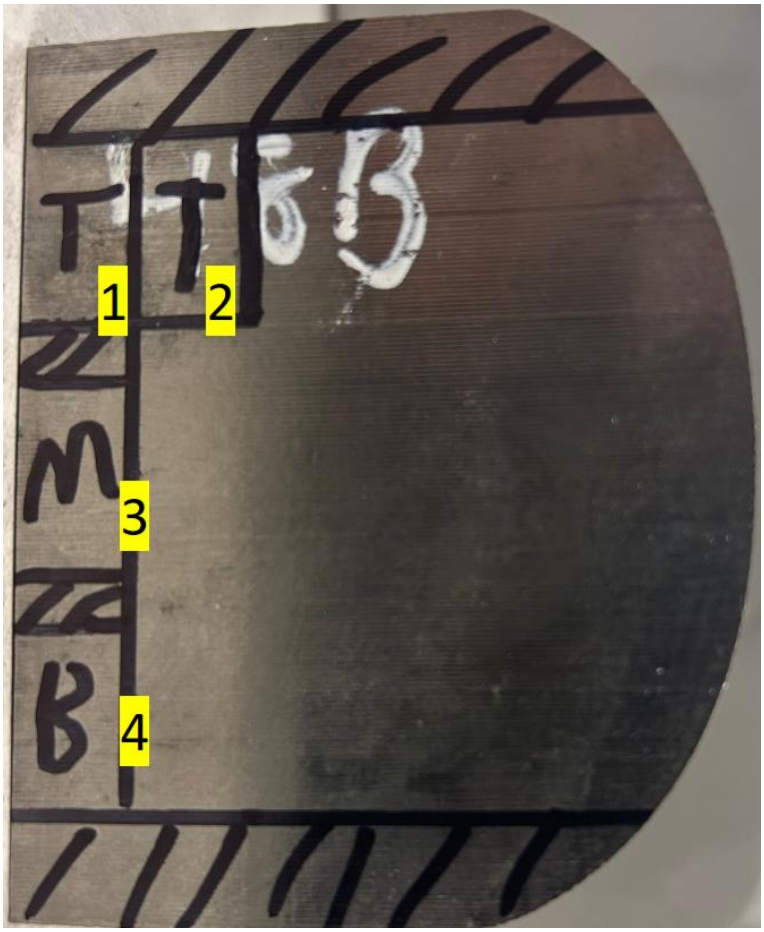

Figure 13. Face of sample 48B with associated markings where samples would be sectioned from: 1) Sample T1, 2) Sample T2, 3) Sample M, and 4) Sample B.

6.2 Cutting and Mounting

6.2.1 Cutting and Mounting of Ti64

The initial approach in preparing the Ti64 samples was based on the assumption that they would require similar sample preparation methods as steel. This turned out to be not an entirely accurate assumption, resulting in many of the sample preparation steps being refined in which trial and error was needed to find the best way to prepare the Ti64 samples for metallographic inspection.

Cutting was performed using a silicon carbide cutoff wheel in a Leco MSX 255™ abrasive saw. A "pulsing" method of cutting was employed where the operator of the abrasive saw alternated between applying light and heavy pressure on the blade during the cut. This was done to reduce work hardening of the Ti64 and therefore make the cut cleaner and faster. Cutting these samples presented some challenges, as cutting larger pieces of the Ti64 sample often resulted in broken blades. However, methods to prevent blade breakage were eventually found. This primarily consisted of preventing the sample from cooling

down to room temperature, as it is believed that allowing the sample to thermally contract led to it clamp onto the blade and break it.

The quarters of the Ti64 billets needed to be cut to size to mount in Bakelite for polishing. A large cut was made in the quartered billet to produce a slice approximately 10 mm thick. This slice was then sectioned into individual samples. First, the top and bottom 9.5 mm of the billet were removed (to remove any surface defects that could have been induced by processing) (Figure 13). 16 mm long samples were then sectioned from the slice (Figure 13). This resulted in two samples from the top of the billet, one sample from the middle of the billet, and one sample from the bottom of the billet from each of two quarters from billets 47 and 48. After cutting these samples from the billets, any burrs were removed using a belt sander with an alumina grit belt. Then an Allied Techpress 2™ automatic mounting press was used to mount each sample in Bakelite. It should be noted that for this project's purpose, the samples are mounted so that a transverse face (i.e., a face of the sample whose normal is perpendicular to the axis of the billet) of the sample is polished. The transverse cross section of the ring will show all surfaces in contact with the forge and die; many of the differences from the hammer process are likely to be most easily distinguished on the surface of the sample.

6.2.2 Cutting and Mounting of INCO 718

Because the Ti64 samples were processed first, it was learned that more preliminary research should be conducted to streamline the processing of the INCO 718 samples. Therefore, sectioning research was conducted, and test cuts on scrap INCO 718 pieces (supplied by CFW) were conducted. This proved the silicon carbide blade was effective in cutting INCO 718.

While the INCO 718 billets had a similar radius to the titanium (~3”), they were much longer (8” vs 4”). Therefore, it was decided that waterjet cutting would be used to make the initial slices in the billet. This decision to use waterjet cutting greatly reduced the time needed to process the INCO 718. The slices were nominally 6.35 mm (0.25”) thick, but limitations in the waterjet setup resulted in slices 4 – 7 mm thick. The same cutting scheme used in the Ti64 was also used in the INCO 718: 9.5 mm of material was removed from the top and the bottom of the billet, followed by 16 mm-long samples sectioned from the top, middle, and bottom of the quarter. Samples were sectioned from this slice using a silicon carbide cutoff wheel in the same Leco MSX 255™ abrasive saw as was used in the Ti64. Due to the thin cross section of the INCO 718 as well as its milder work hardening behavior, sectioning INCO 718 was straightforward and required no pulsing of the cutoff wheel.

After cutting these samples from the billets, any burrs were removed using a belt sander with an alumina grit belt. Then an Allied Techpress 2™ automatic mounting press was used to mount each sample in Bakelite. The same transverse mounting process used for Ti64 was used for INCO 718.

6.3 Grinding and Polishing

6.3.1 Grinding and Polishing of Ti64

Grinding the samples consisted of using a series of silicon carbide papers of increasing grit number: 240, 320, 480, and 600. It was found that applying heavy pressure and slow speeds was most effective in grinding the samples. This helped prevent rounding of the sample and proved to be quicker.

Fine polishing was attempted using a series of polishing wheels with diamond polishing solution of varying grit sizes: 6 μm, 3 μm, 1 μm, and 0.05 μm. When this did not yield satisfactory results (i.e., when significant surface roughness and scratching were observed), a different method of chemical mechanical abrasion was used. This method used a 9 μm diamond solution polish followed by polishing with 0.05 colloidal silica in 30 wt% hydrogen peroxide. Polishing with the 9 μm diamond solution was used until all scratches from grinding were no longer visible. The polishing step using 0.05 μm silica in the hydrogen peroxide solution was used for 8 minutes in a counter rotation to the polishing wheel followed by 2 minutes of static polishing on the wheel. This resulted in a mirror finish on the sample; inspection of the sample at 200X magnification using a light microscope confirmed that this polish was sufficient for etching. This polishing method even revealed some grains, although they were not defined enough to reliably count without etching.

6.3.2 Grinding and Polishing of INCO 718

Grinding the samples consisted of using a series of silicon carbide papers of increasing grit number: 240, 320, 480, and 600. It was found that medium pressure and medium speeds was most effective in grinding the samples. It was also found that the INCO 718 was very soft and sensitive to scratching.

Fine polishing was accomplished using a series of polishing wheels with diamond polishing solution of varying grit sizes: 9 μm, 3 μm, 1 μm, finishing with a 0.05 μm alumina solution. Polishing times varied depending on the thickness of the sample, and microscopy was used to check whether each polishing step was sufficient. This resulted in a mirror finish on the sample; inspection of the sample at 200X magnification using a light microscope confirmed that this polish was sufficient for etching.

6.4 Etching

6.4.1 Etching of Ti64

The etchant used for the Ti64 samples was Kroll's reagent. This etchant is a hydrofluoric acid (HF) and nitric acid-based etchant. It is regarded to be the industry standard for etching titanium-based alloys for metallographic purposes. Because of the HF in the reagent, great caution was employed in using Kroll's reagent. Personal protective equipment (PPE) included wearing long pants, closed-toe shoes, polycarbonate safety glasses, a polycarbonate face shield, nitrile gloves, neoprene over-gloves, and a chemically resistant lab apron with sleeves. Calcium gluconate gel was available within arm's reach at all times when using this reagent.

The etchant was applied to the samples using a cotton swab and was left for 5 minutes undisturbed. Then the samples were rinsed off with tap water and all contaminated glassware was washed with water; all HF-containing water was properly disposed of in a high-density polyethylene (HDPE) hazardous waste container. Although HF can etch glassware, it was deemed unnecessary to use HF-compatible polymer labware due to the low concentration of HF in Kroll's reagent and the short time of exposure of the glassware to the etchant.

After etching, preliminary examination of the sample surface using a light microscope was performed to confirm proper etching of the sample. If the sample seemed under etched (i.e., grain boundaries not properly or fully defined), it would be etched for one additional minute. If the sample appeared over etched (i.e., significant discoloration or visible deep corrosion of the sample), then final polishing would be conducted on the sample again to prepare it for re-etching.

6.4.2 Etching of INCO 718

The etchant used for the INCO 718 samples was Kalling's reagent. This etchant is a cupric chloride and hydrochloric acid-based etchant. This was far less hazardous when compared to the Kroll's reagent used in the Ti64 etching, so the PPE needed was less extensive. The PPE included wearing long pants, closed-toe shoes, polycarbonate safety glasses, nitrile gloves, and a chemically resistant lab apron with sleeves.

Determining an optimal exposure duration of the reagent took several attempts, and it was found that a 3 minute exposure to the reagent was the most effective. It also took several trials to find the best method of applying the reagent to the sample. Swabbing the sample with a cotton-tipped swab resulted in scratches on the sample, and immersion of the sample in the reagent was not considered due to its

inefficient use of etchant and safety concerns. A pipette method where etchant was pipetted onto the sample surface without contacting it was used and proved to be highly effective. Then the samples were rinsed off with water and all contaminated glassware was washed with tap water; all etchant-containing water was properly disposed of in a high-density polyethylene (HDPE) hazardous waste container.

After etching, preliminary examination of the sample surface using a light microscope was performed to confirm satisfactory etching of the sample. If the sample seemed under etched (i.e., grain boundaries not properly or fully defined), it would be etched for one additional minute. If the sample appeared over etched (i.e., significant discoloration or visible deep corrosion of the sample), then final polishing would be conducted on the sample again to prepare it for re-etching.

6.5 Sample Imaging

6.5.1 Sample Imaging of Ti64

Samples were imaged using a Leica inverted light microscope. Having smooth, unrounded surfaces on the polished and etched samples were crucial for obtaining useful images. After all of the samples were imaged, the artificial intelligence (AI) image analysis software “MIPAR” was originally chosen to measure grain size, but it proved ineffective. This was likely due to the data set that the AI was trained on being significantly different from the images that we collected. As a result of this, the software could not accurately identify grain boundaries in our sample. It was then decided to measure grain size by hand using the ImageJ software. After loading the images into the software and setting their size scales, two different grain size measurement techniques were used. The first method to determine an average grain size was the ASTM E112-13 line intercept method. This consists of randomly drawing a line on the microstructure and counting how many times it intercepts a grain boundary. 20 lines were drawn per sample and compiled to determine an average grain size for the whole billet. Minor and major axis measurements of individual grains were made by drawing straight lines from one end of a grain to the other along the major and minor axes (Figure 14). For each sample, 200 – 300 grains were measured at random, and used to plot the distribution of grain sizes. This second method was chosen to display the distribution of grain sizes, as the line intercept method is an average value.

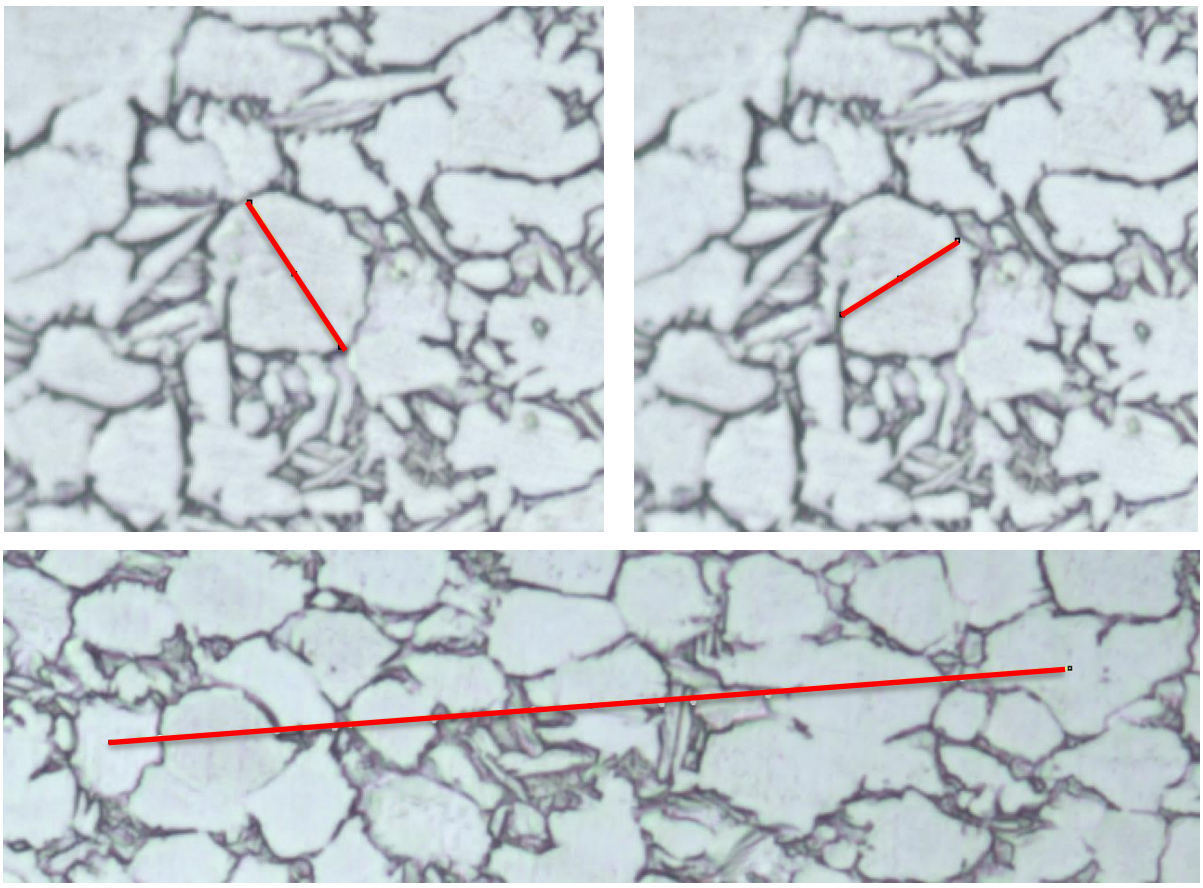

Figure 14. Illustration of major and minor axis measurements of grain size (top). Average grain size by ASTM E112-13 line intercept (bottom).

6.5.1 Sample Imaging of INCO 718

Samples were imaged using a Leica inverted light microscope. After all of the samples were imaged, grain size was measured using the ImageJ software. After loading the images into the software and setting the size scales, the ASTM E112 Hilliard single circle method was used to measure the average grain size. This method consists of applying a circle (whose diameter is no smaller than the diameter of the largest grain in the image) onto each image, calculating the circumference of this circle, counting the number of grains that intersect the circumference of the circle, and dividing the circumference by the number of grains intersecting it to obtain an average grain size for that image. This method was used as ASTM recommends using grain intercepts with a circle (rather than grain intercepts with a line) for grains that are not equiaxed. If applied to the INCO 718 microstructure, single line intercept methods of measuring average size would result in an inconsistent measurement. For example, if the line traversed a twin boundary, the result would be a small grain size, but if the line aligned along the twin boundary, the

grain size would be much larger. Therefore the Hilliard single circle method seemed to be appropriate method for measuring average grain size in INCO 718 given the high degree of twinning that was observed in the INCO 718 samples. Applying this procedure to the INCO 718 images appeared to give a good mix of large grains, twinned grains, and small necklace grains intersecting the circle. For each sample, 10 images were counted, from the bottom to the top of the sample. When capturing the image, care was taken to have the bottom of each field match the top of the previous image (so that if the images were stitched together, they would form one continuous image from the bottom to the top of the sample). This left room for error, however, as there was difficulty in aligning the photos perfectly. Because of this, the location in the billet where each photo was taken could not be determined.

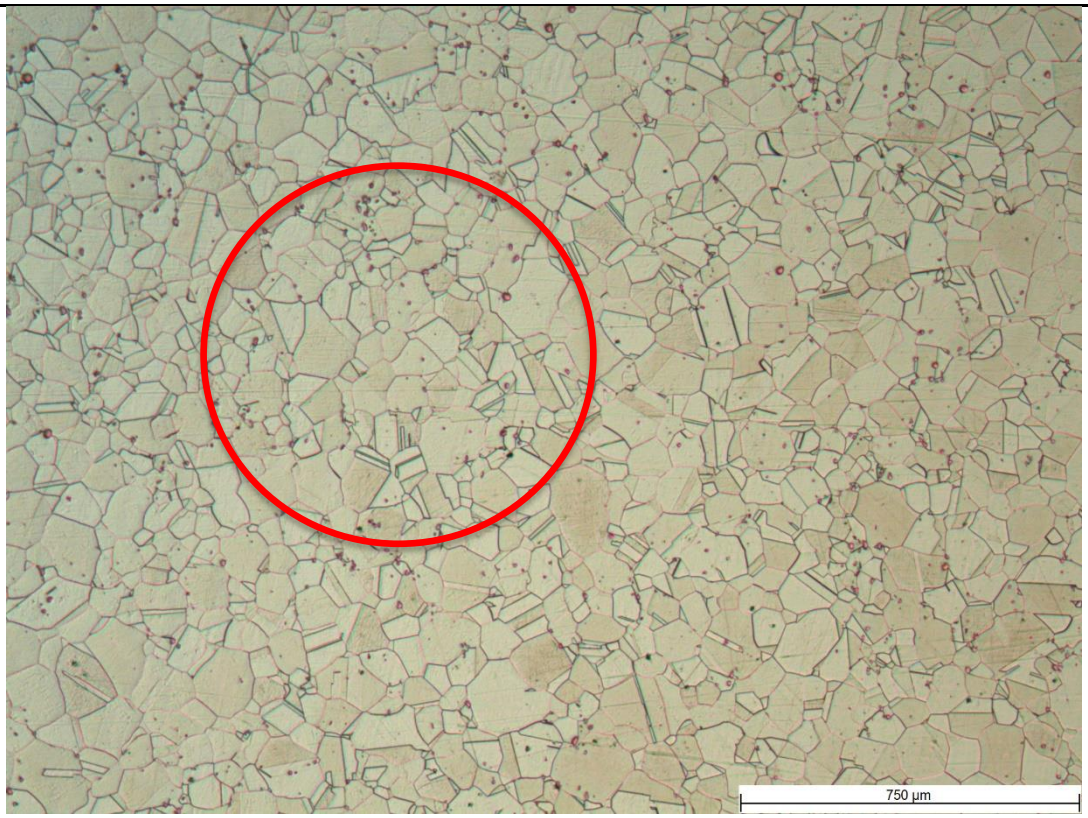

Figure 15. Illustration of ASTM E112-13 Hilliard single circle method for measuring average grain size.

7. Results and Discussion

7.1 Results and Discussion of Ti64

7.1.1 Grain Size Measurements

Table 1 shows the average grain size and standard deviation in grain size determined using the ASTM E112-13 line intercept method for each sample. For every sample that was imaged, grain size measurements were taken from random locations in the image and from 3 – 5 images of the sample to avoid bias. Figure 16 shows the distribution of grain size measurements across all samples from each billet. Sample naming follows an X-Y-Z convention:

- X denotes the billet number,
- Y denotes the quarter of the billet, and
- Z denotes the location of the sample in the quarter (T1 and T2 denote samples taken from the top, M denotes samples taken from the middle, and B denotes samples taken from the bottom).

Table 2 shows the overall average grain size and standard deviation in grain size (based on data from Table 1) for each Ti64 billet. These values show only a small difference in average grain size between the billets that is not statistically significant, as the difference in average grain size is considerably smaller than the standard deviation in grain size.

Table 1. Average grain size and standard deviation of grain size in the Ti64 samples.

Sample	Average Grain Size (μm)	Standard Deviation (μm)
47-A-T1	9.83	2.40
47-A-T2	9.26	2.72
47-A-M	9.65	3.57
47-A-B	10.20	3.21
47-C-T1	9.68	3.23
47-C-T2	10.05	2.97
47-C-M	9.21	3.31
47-C-B	9.83	2.02
48-C-T1	8.98	2.90
48-C-T2	9.39	3.16
48-C-M	9.05	3.78
48-C-B	9.55	2.98
48-D-T1	10.46	2.81
48-D-T2	9.57	2.79
48-D-M	9.88	3.66
48-D-B	10.11	3.41

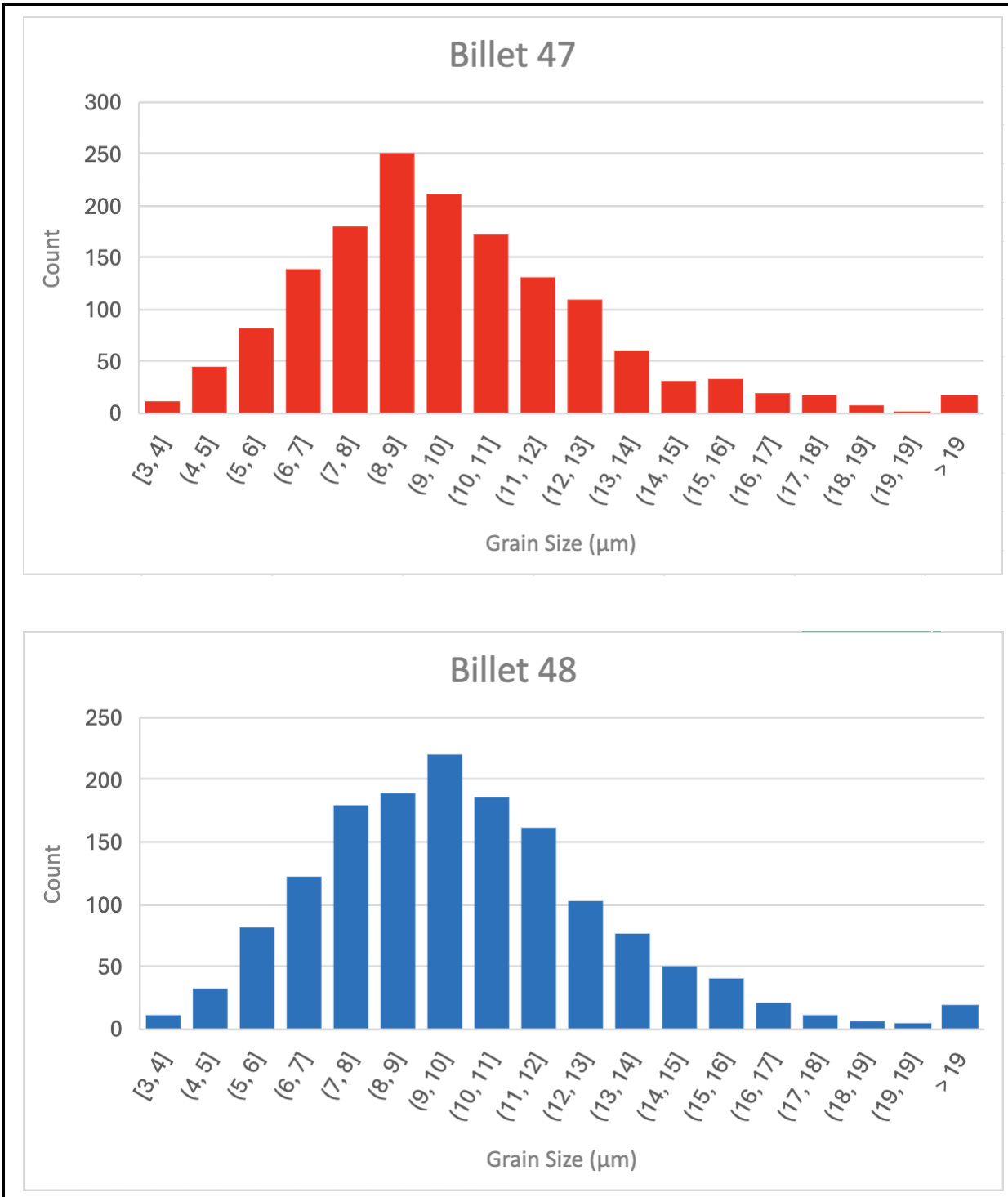

Figure 16. Histograms displaying the distribution of grain sizes in billets 47 and 48.

Table 2. Average grain size for each of billet 47 and billet 48.

Billet	Average Grain Size (μm)	Standard Deviation (μm)
47	9.77	1.66
48	9.76	2.16

A t-test was applied to the grain size data. The t-test tests the hypothesis that two sets of data have statistically significant different means. If the p value from the t-test is below 0.05, the null hypothesis that the two billets have the same average grain size is rejected. The p value for the two tailed t-test (assuming the same variance) was 0.44. Because this is much higher than our confidence interval of 0.05, the null hypothesis is not rejected. Therefore there is no statistically significant difference between the average grain sizes of the two billets. Hence it can be concluded that hammer forging and hydraulic press forging makes no difference in the average grain size in Ti64.

7.1.2 Sample Images

A key part of our investigation of Ti64 was visual observation and comparison of the microstructure between billets. It should first be noted that our polishing and etching technique became more refined as we continued. Having first started with billet 47, our samples and therefore our images from billet 48 are of higher quality and show more well-defined microstructure features. These differences are apparent in our images (Figures 17 and 18), but did not impede accurate measurement of grain size. Aside from slight quality differences in the polishing and etching of the samples, the microstructures between billet 47 and 48 appeared similar based on grain size measurements and visual comparison.

7.1.3 Notable Microstructure Features

When imaging the microstructure of billet 48 samples, there were a few features that stood out from the homogeneous microstructure. Figure 19 shows an agglomeration of alpha grains that clearly stand out from the surrounding microstructure. Highly elongated bright alpha grains were observed that are also slightly wider than the surrounding grains. These were surrounded by a much larger area of the dark beta phase. These agglomerations were observed across multiple samples from both billets 47 and 48 and were not of concern to CFW. Figure 20 shows an extremely elongated alpha grain, measuring around 400 μm in length. This was the only such instance of a grain with such an unusual length; this was also not a concern to CFW. All the microstructural features noted above were aligned along the axis from the bottom to the top of the billet. These features are most likely a result of either the raw unprocessed material, or the results of pre-forming heat treatments performed before the billets reached CFW for final shaping, and therefore unlikely to be a result of a difference between forging methods.

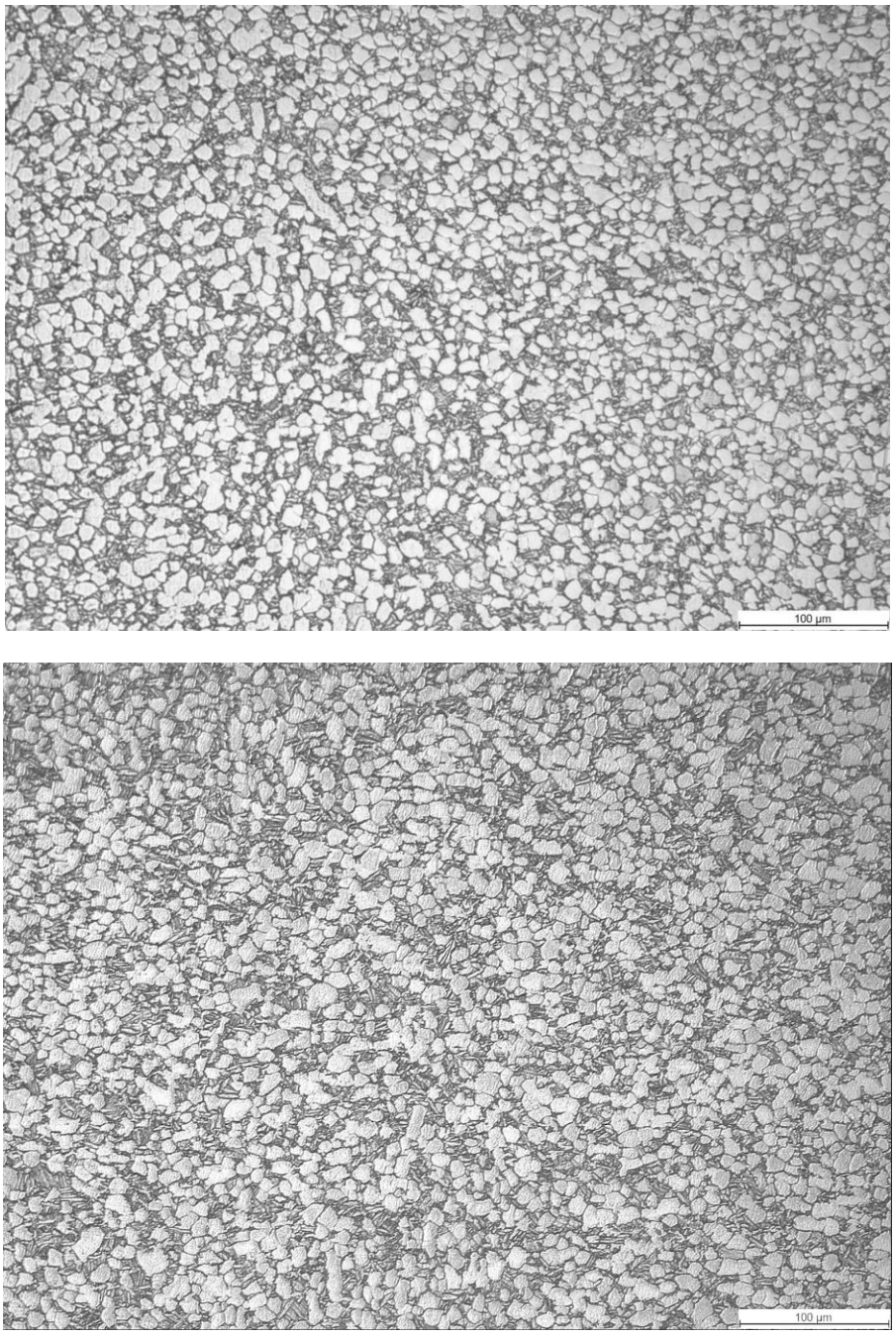

Figure 17. Light microscope images comparing the microstructures of billets 48 and 47: (top) sample 48-D-B and (bottom) 47-C-B.

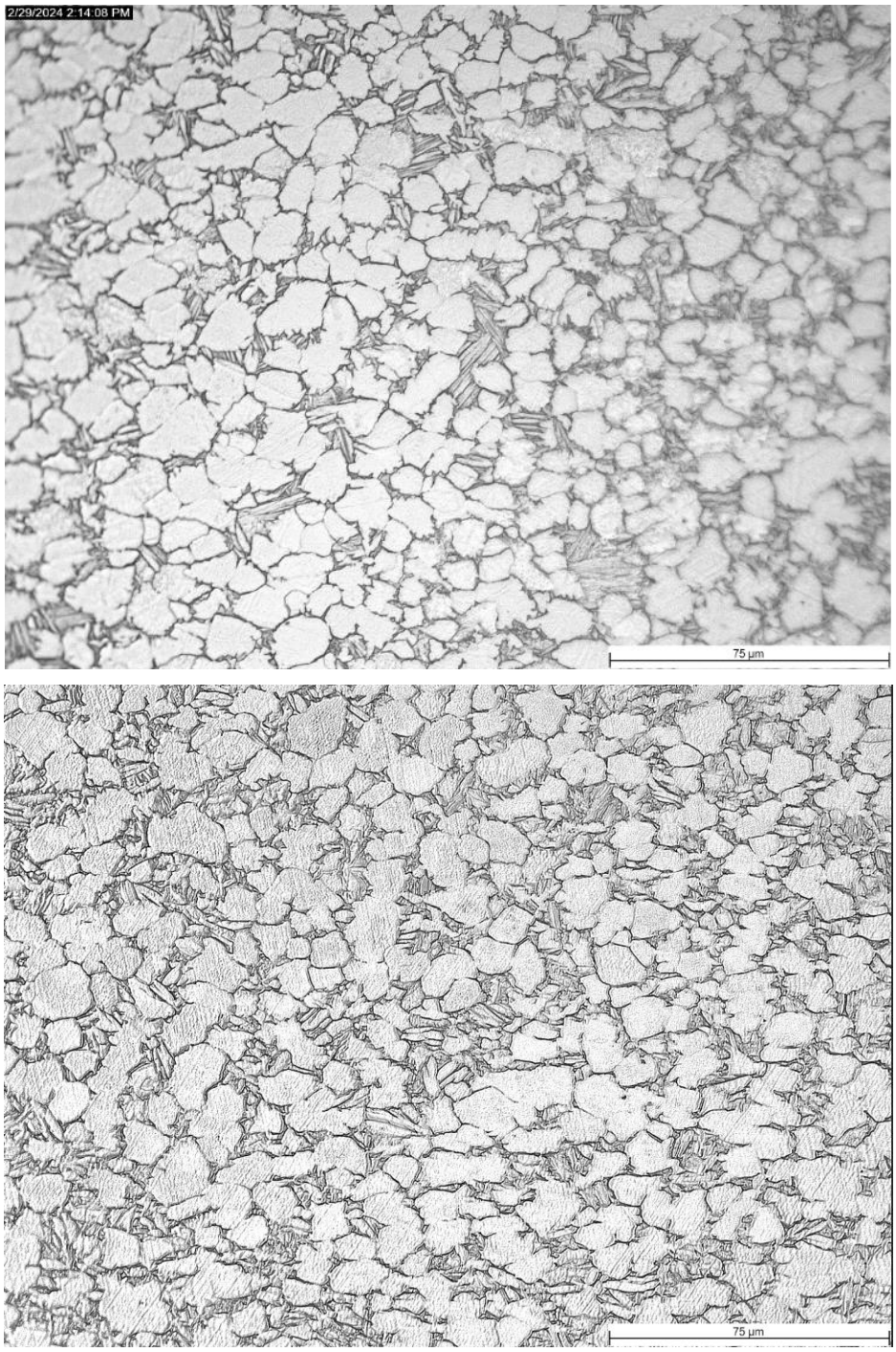

Figure 18. Light microscope images comparing the microstructures of billets 48 and 47: (top) 48-C-T1 and (bottom) 47-C-T1.

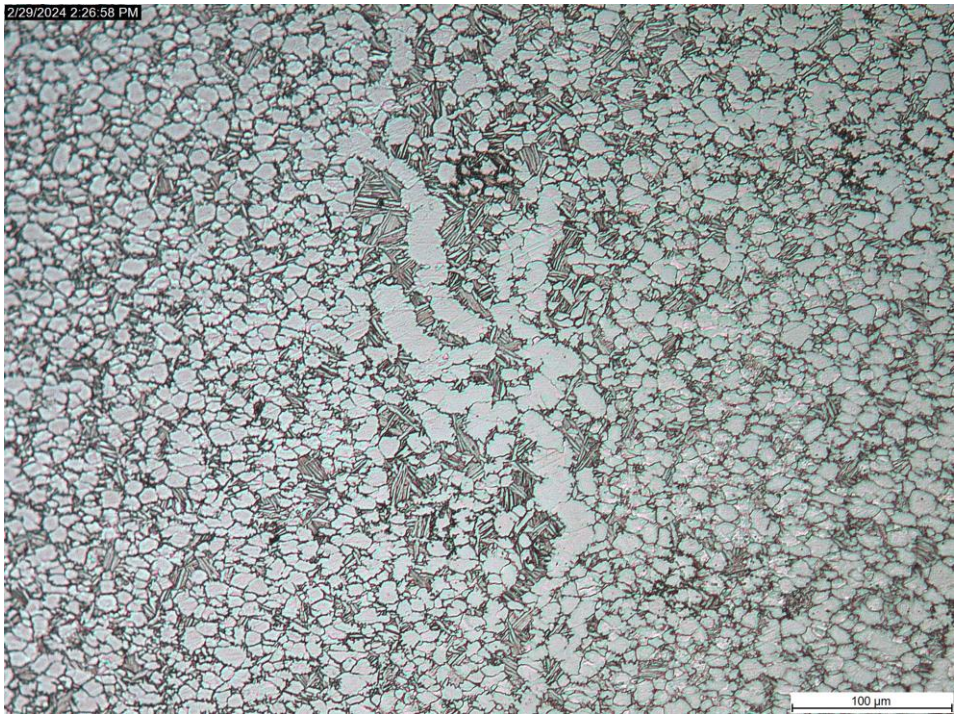

Figure 19. Light microscope image of sample 48-D-M showing agglomeration of the alpha phase.

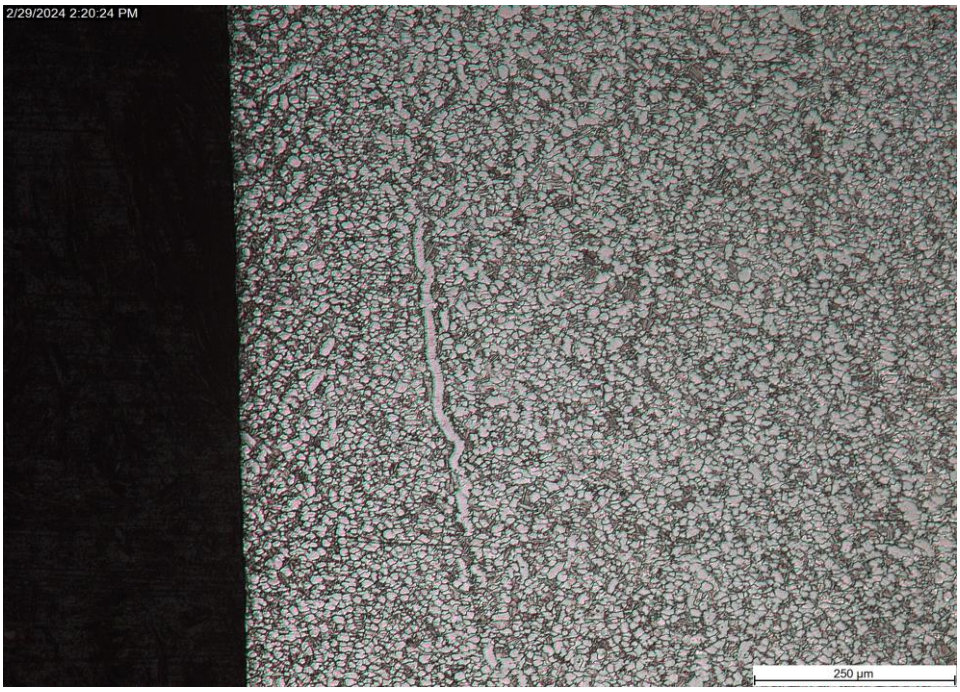

Figure 20. Light microscope image of sample 48-D-M at showing an elongated alpha grain roughly 400 µm in length.

7.1.4 Hardness

To confirm whether there was any difference between the forging methods, mechanical property measurements were made in addition to the microstructural analysis. In lieu of yield testing (due to the difficulty of fabricating test samples), hardness testing was conducted. Hardness testing was conducted on the top, middle, bottom, and edge of the samples (Figure 21). Three Rockwell C hardness measurements were made in each of these regions with a Wilson® Rockwell® 2000 Hardness Tester. Because two samples were available from each billet, a total of 6 hardness measurements were taken for each region in each billet. As seen in Table 3, the hardness between the billets is similar, but billet 48 is consistently slightly harder than billet 47 in all regions (Figure 22).

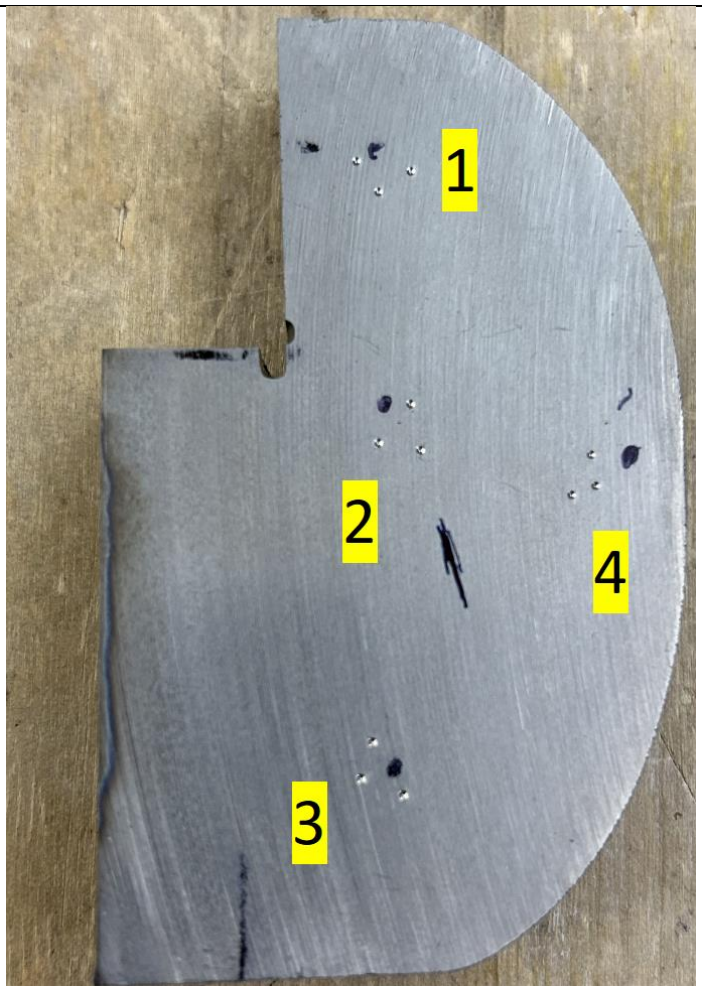

Figure 21. Sample 48-A hardness testing indentation locations: 1) Top region, 2) middle region, 3) bottom region, and 4) edge region.

Table 3. Rockwell C hardness data from billets 47 and 48.

Sample	Average Hardness (HRC)	Standard Deviation
47 Top	31.3	0.56
47 Middle	31.7	1.19
47 Bottom	33.9	1.26
47 Edge	34.3	2.35
48 Top	34.9	0.85
48 Middle	33.2	0.83
48 Bottom	34.5	0.41
48 Edge	35.1	0.53

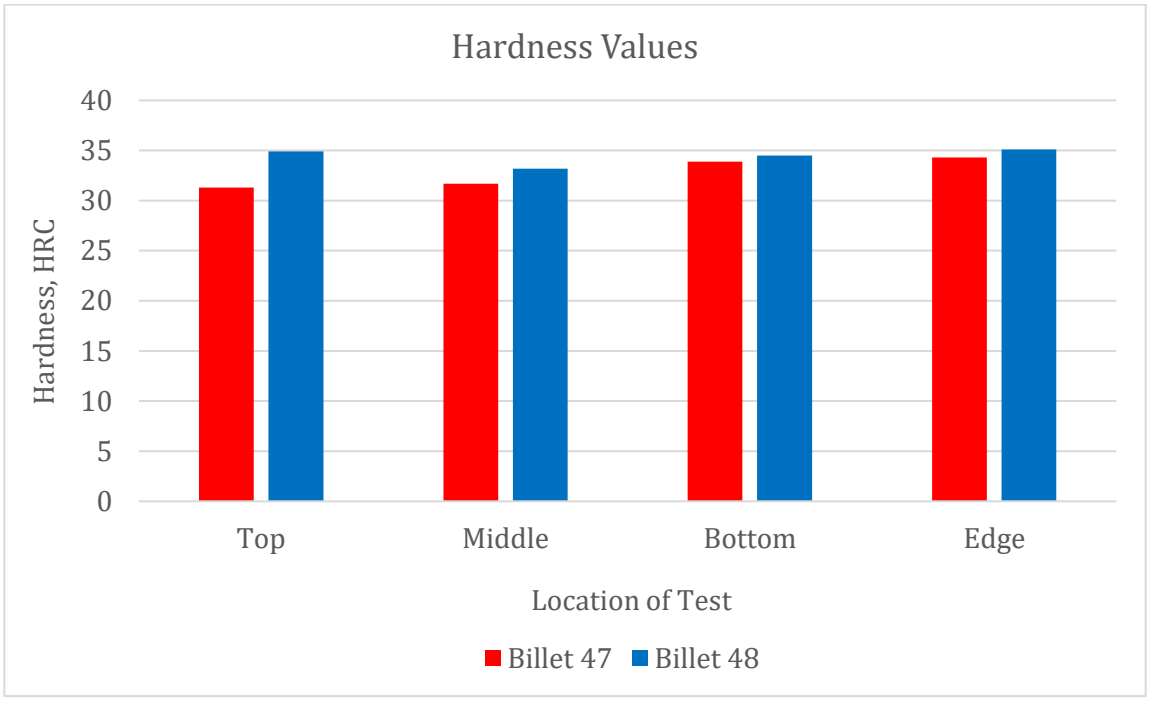

Figure 22. Comparison of hardness values between billets 47 and 48.

To compare the average hardness values for each sample, a t-test was performed. In this case, the null hypothesis is that there is no difference in average hardness value between the two billets. With an alpha of 0.05, if the p value is lower than 0.05, the null hypothesis is rejected. The null hypothesis in this

test is that the two billets have the same hardness. Alpha is the probability of rejecting the null hypothesis when the null hypothesis is true; when alpha is lower, the result is more certain. The p value of the two tailed t-test (assuming unequal variance) was 0.0001. With this, the null hypothesis is rejected; billet 48 is harder than billet 47. It is recommended that this result be confirmed with further hardness testing.

Based on these observations and the analysis of grain size data obtained for the Ti64 billets, we hypothesized that billet 47 was hammer forged, and billet 48 was hydraulic press forged. With only very small differences between the two billets our hypothesis was formed based on the thought that the hammer forge would be more likely to break up the large grains that we saw in billet 48.

7.2 Results and Discussion of INCO 718

7.2.1 Grain Size Measurements

It should first be noted that the grain size was observed to change significantly when progressing outward from the middle region of the billet to the top or bottom surface of the billet. Grains near the surface were larger and oblong, while grains in the middle were smaller and equiaxed. Because of these location-dependent differences in grain size and shape, only samples from the middle region of each INCO 718 billet were used in grain size comparison. The average grain size of billet 43 was found to be significantly lower than that of billet 44 (Table 4). Billet 43 has a larger standard deviation in its grain size, but this difference in standard deviation between billets is relatively small.

Table 4. Average grain size for middle samples in each of billet 43 and billet 44.

Billet	Average Grain Size (μm)	Standard Deviation (μm)
43	41.86	5.057
44	49.57	4.618

An ANOVA test was applied to the grain size data. The ANOVA test tests the hypothesis that the two sets of data have statistically significant different means. If the p value from the t-test is below 0.05, the null hypothesis that the two billets have the same average grain size is rejected. The p value for the ANOVA test was 0.00196. Because this is less than our confidence interval of 0.05, the null hypothesis is rejected. Therefore, there is a statistically significant difference between the average grain sizes of the two billets. Hence it can be concluded that hammer forging and hydraulic press forging make a difference in the average grain size of INCO 718, leading to smaller grains in billet 43.

7.2.2 Grain Size Distribution

An important consideration throughout the analyses of the average grain size and grain size distribution of the INCO 718 billets is how the grain sizes and shapes change depending on location with the billet. Samples taken from the top, middle, and bottom regions all showed differences in grain size (Figure 23). This difference is most pronounced over the entire height of the billet, but individual samples from the top and bottom regions were also affected by this change of grain size. Within a single sample from either the bottom or top regions, grain sizes vary from ~40 μm to ~100 μm. The largest grains are seen closest to the surface of the billet, and the grain size decreases towards the middle of the sample (Figure 24). This grain size change within the sample proved to be an obstacle in the analysis of the grains. As specified in the ASTM E112-13 Hilliard single circle method, only one grain measurement can be taken from each image. Given 10 images per sample (taking photos from the bottom to the top of the sample), this results in every image having a different grain size. Because of this, a mean grain size for the sample calculated by averaging the grain size from each photo had little significance. This led to all top and bottom region samples being useful for qualitative analysis, but not contributing to the quantitative analysis.

It is believed that the grain size and shape changes are due to uneven cooling of the billet during forging. The middle of the billet would stay at high temperatures long enough to allow for a high degree of recrystallization. This results in a microstructure akin to an annealed condition. By comparison, the surface of the billet cooled much more rapidly due to greater exposure to the atmosphere and metal surfaces (which can dissipate heat quickly) during forging operations. This effect would be more pronounced in INCO 718 than in Ti64, as the thermal conductivity of INCO 718 is about 70% higher than that of Ti64 (11.4 W/m-K for INCO 718 versus 6.4 W/m-K for Ti64 [14]). It is theorized that this faster cooling at the billet surface did not allow grains near the surface of the billet to recrystallize into equiaxed grains, resulting in larger unrecrystallized grains [38]. Another contributing factor to this uneven heating is the friction of the billet surface and the hammer or hydraulic forge press; there is a potential for the extra heat energy added from the process to allow further grain growth. This could be exacerbated by the fact that the furnace heats the billet from the surface to the center; the high heat transfer rate at the surface of the billet may have led to the greater grain size at the surfaces of the billet.

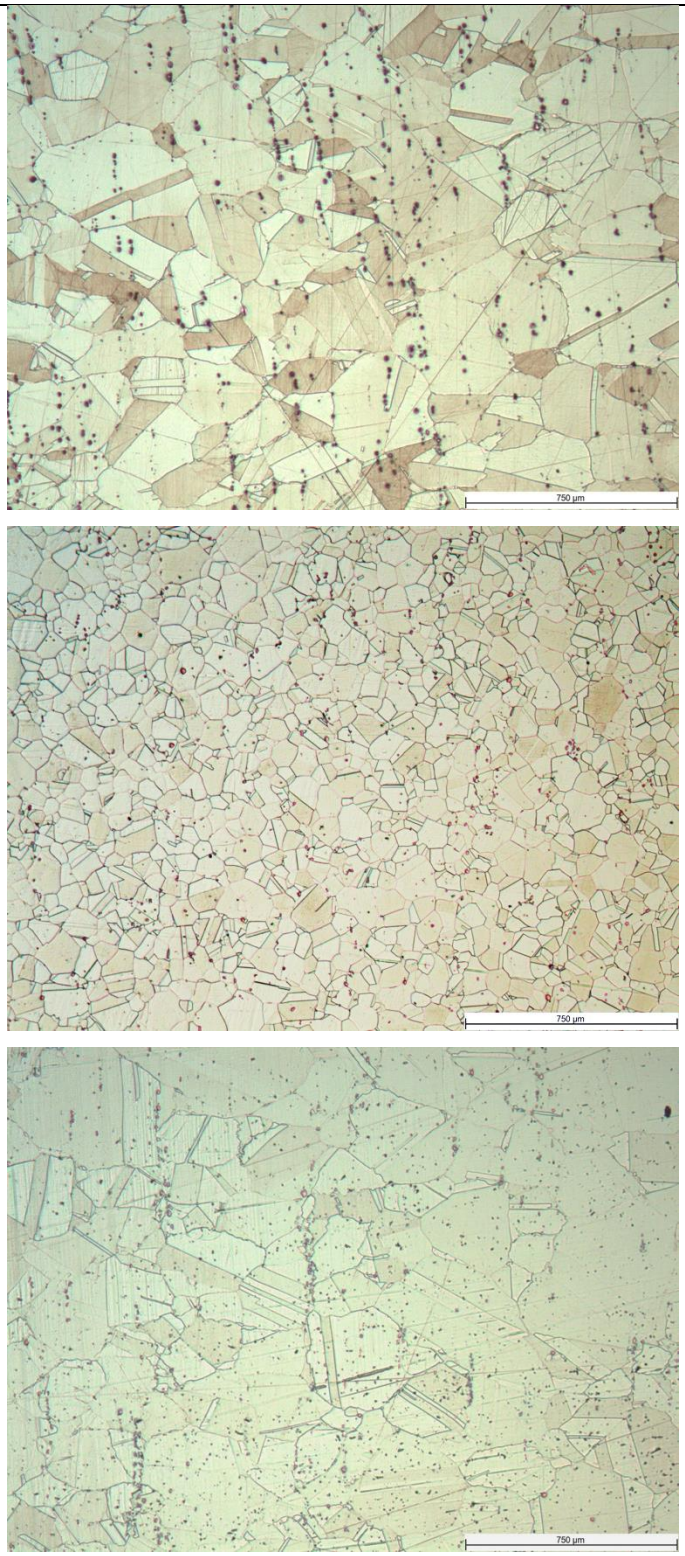

Figure 23. Visual comparison of multiple samples from billet 43 showing change in grain structure in top, middle, and bottom regions of the billet.

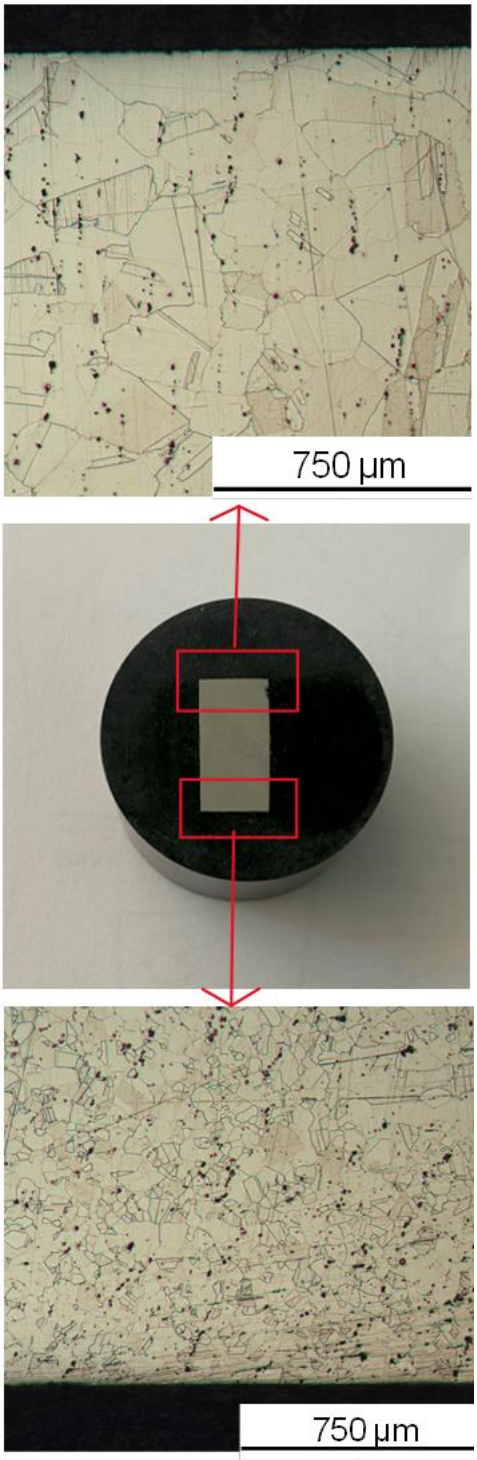

Figure 24. Sample 43-A-T1 showing grain size changes through the height of the sample

7.2.3 Necklace Grains

Necklace grains are smaller (~10 μm) grains that surround larger (~100 μm) grains, typically along grain boundaries. Top region samples from billet 44 showed a large amount of necklace grains (Figure 25). No samples from billet 43 showed evidence of necklace grains, regardless of sample region. Because necklace grains are small grains located along grain boundaries, it can be reasonably concluded they nucleated separately from the larger grains and did not have adequate time at recrystallization temperatures to grow larger. The extra energy needed to nucleate these necklace grains could have come from the high strain rates associated with hammer forging. This could also explain why these are seen in the top region samples and nowhere else in the billet. Based on these observations and the analysis of grain size and grain shape data obtained for the INCO 718 billets, we hypothesized that billet 44 was hammer forged, and billet 43 was hydraulic press forged. This hypothesis was especially influenced by the presence of necklace grains in billet 44.

7.2.4 Hardness

Similar to Ti64, hardness testing was conducted. Hardness testing was conducted on the top, middle, bottom, and edge of the INCO 718 samples, identical to the process used for Ti64 (Figure 21). Five Rockwell C hardness measurements were made in each of these regions with a Wilson® Rockwell® 2000 Hardness Tester. Because only one sample was available from each billet, a total of 5 hardness measurements were taken for each region in each billet. As seen in Table 5 and Figure 26, the hardness differences between the INCO 718 billets varies depending on location in the sample.

To compare the average hardness values for each sample, a t-test was performed. In this case, the null hypothesis is that there is no difference in average hardness value between the two billets. With an alpha of 0.05, if the p value is lower than 0.05, the null hypothesis is rejected. The null hypothesis in this test is that the two billets have the same hardness. Alpha is the probability of rejecting the null hypothesis when the null hypothesis is true; when alpha is lower, the result is more certain. The p value of the two tailed t-test (assuming unequal variance) was 0.146. With this, the null hypothesis cannot be rejected; it is unknown which billet is harder overall. A single factor ANOVA test was applied to solely the hardness measurements from the middle of each billet with an identical null hypothesis and alpha as the previous test. This resulted in a p value of 0.009, with this, the null hypothesis is rejected. The middle region of billet 43 is harder than the middle region of billet 44. This matches the grain size indications; smaller grains are associated with higher hardness.

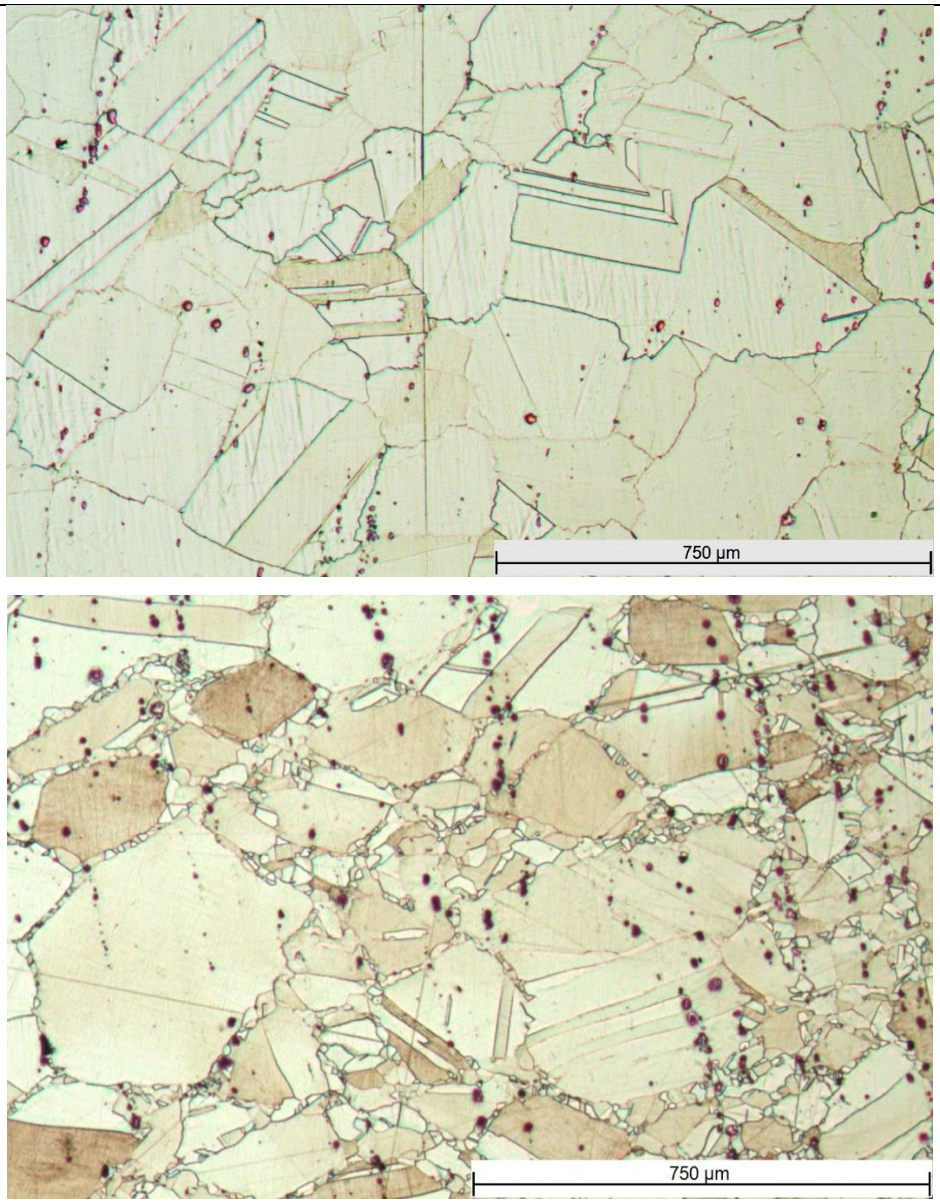

Figure 25. Visual comparison between (top) sample 43-A-T1 with no necklace grains, and (bottom) sample 44-A-T2 which shows necklace grains.

Table 5. Rockwell C hardness data from billets 43 and 44.

Sample	Average Hardness (HRC)	Standard Deviation
43 Top	30.40	2.71
43 Middle	29.70	0.95
43 Bottom	30.32	0.83
43 Edge	31.52	0.53
44 Top	31.24	1.32
44 Middle	26.54	1.15
44 Bottom	32.16	0.85
44 Edge	29.34	1.26

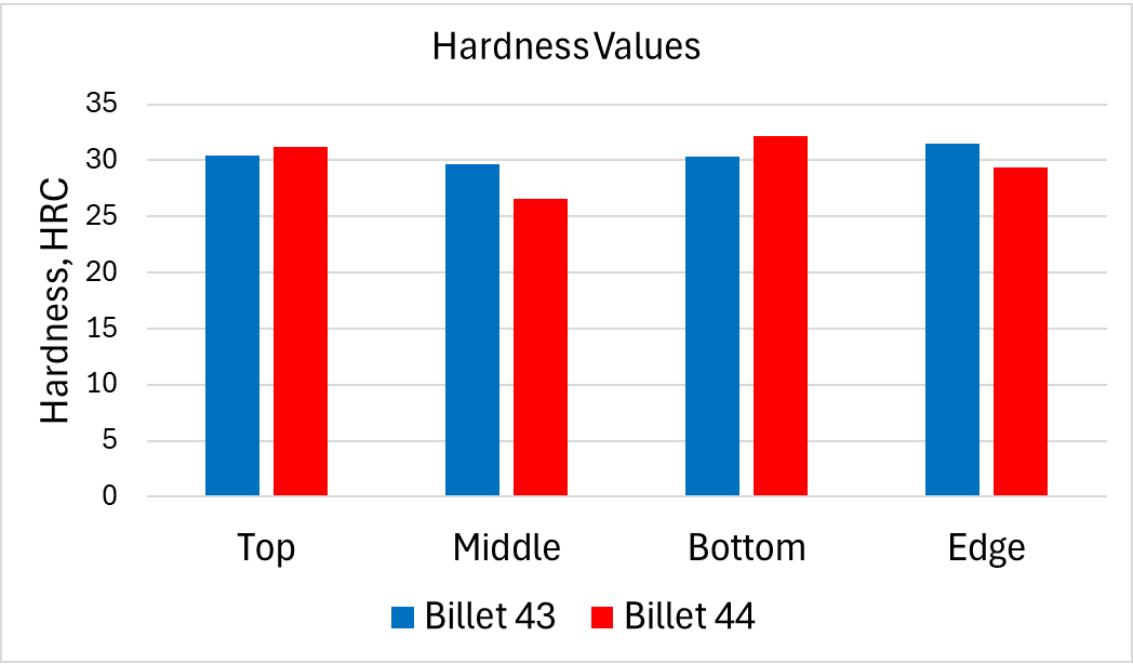

Figure 26. Comparison of hardness values between billets 47 and 48.

8. Billet Identification

After completing the results of our report and consulting with the project sponsor (Carlton Forge Works), each billet was identified with its corresponding forging process allowing us to draw conclusions as to how each forging method influenced the microstructure and properties of each alloy (Table 6).

Table 6. Billet and process identification.

Alloy	Billet	Process
Ti64	47	Hydraulic Press
	48	Hammer Forge
INCO 718	43	Hydraulic Press
	44	Hammer Forge

9. Conclusions

Ti64

1. Numerical and visual data show no statistically significant indication that the type of forging method influences the microstructure of Ti64 produced at CFW.
2. More research is likely needed to determine whether the type of forging method influences the hardness of each billet. Current data shows that hammer forged samples have higher hardness.

INCO 718

1. Numerical and statistical analysis show a smaller grain size in the hydraulic forged samples.
2. Grains become dramatically larger when approaching the surface of the billet for both hydraulic forging and hammer forging.
3. Necklace grains are more common in the top region of the billet in hammer forged samples.
4. Hardness varies with location in the sample. In particular, hardness was higher in the middle of the INCO 718 billets, which is consistent with the presence of the small necklace grains in the middle of the billets.

10. Future Work

Ti64

1. Continue hardness testing to confirm a hardness difference between hydraulic press forged and hammer forged Ti64 billets

INCO 718

1. Expand analysis of middle region samples to confirm hardness and grain size difference
2. Establish method to measure location of sample photos within billet for quantitative analysis to relate grain size to location in billet

Other Alloys

Conduct metallography investigation comparing hammer forge and hydraulic press forge on other alloys use by CFW, such as 17-4 PH stainless steel and a 2000 series aluminum.

11. Acknowledgements

Project Sponsor - Joe Redfearn – Associate Manager of Metallurgy, Carlton Forge Works LLC

Project advisor – Dr. Jean Lee

Student Assistant - Jack Coker

Department Technician - Eric Beaton

12. References

[1] M. Rathi and N. Jakhade, “An Overview of Forging Processes with Their Defects”, *International Journal of Scientific and Research Publications*, vol. 4, no. 6, 2014.

[2] P. Moorey, “The Archaeological Evidence for Metallurgy and Related Technologies in Mesopotamia, c. 5500-2100 B.C.”, *Iraq, vol.* 44, no. 2, p. 12-38, 1982. https://doi.org/10.2307/4200150

[3] H. Maryon, “Metal Working in the Ancient World”, *American Journal of Archaeology*, vol. 53, no. 2, p. 93-125. 1949. https://doi.org/10.2307/500498

[4] M. Shirgaokar, “Forging Processes: Variables and Descriptions”, *ASM Technical Books: Cold and Hot Forging.* 2005. https://doi.org/10.31399/asm.tb.chffa.t51040007

[5] A. Bhaduri, “Forging: Mechanical Properties and Working of Metals and Alloys”, *Springer Series in Materials Science*, vol. 264, 2018. https://doi.org/10.1007/978-981-10-7209-3

[6] G. Shen, and D. Furrer, “Manufacturing of Aerospace Forgings”, *Journal of Materials Processing Technology*, vol. 98, no. 2, p. 189-195, 2000. https://doi.org/10.1016/S0924-0136(99)00198-3

[7] C. Polu, “Design for Manufacturing: *A Structured Approach*”, *Elsevier Science & Technology Books* p. 241-244, 2001.

[8] A. Tofil and Z. Pater, “Overview of the Research on Roll Forging Process”, *Advances in Science and Technology*, vol. 11, no. 2, p. 72-86, 2017. DOI: 10.12913/22998624/70645

[9] J. Becker, “Open-Die Forging and Preforming Methods", *Forging Equipment, Materials, and Practices.* 1973.

[10] M. Chandrasekaran, “Ch. 9 Forging of Metals and Alloys for Biomedical Applications”, *Metals for Biomedical Devices, Woodhead Publishing*, p. 235-250, 2010.
https://doi.org/10.1533/9781845699246.3.235

[11] T. Altan, and V. Nagpal, “Impression and Closed-Die Forging”, *International Metals Review*, vol. 22, no. 1. 1977. https://doi.org/10.1179/imtr.1977.22.1.322

[12] V. Bhoyar and S. Umredkar, “Manufacturing Processes Part II: A Brief Review on Forging”, *International Journal of Innovation in Engineering and Science*, vol. 5, no. 1, 2010. doi:10.13140/RG.2.2.14162.71365

[13] J. C. Williams and R. R. Boyer, “Opportunities and issues in the application of titanium alloys for aerospace components”, *Metals*, vol. 10, no. 6, p. 705, 2020. *doi:10.3390/met10060705*

[14] “Ansys Granta: Materials Information Management,” *Ansys Granta*. https://www.ansys.com/materials, Accessed Nov. 13, 2023.

[15] R. R. Boyer, “Aerospace applications of Beta Titanium Alloys”, *Journal of Materials*, vol. 46, no. 7, p. 20–23, 1994. doi:10.1007/bf03220743

[16] F. H. Froes, *Titanium: Physical Metallurgy, Processing, and Applications*. Materials Park, OH: ASM International, 2015.

[17] M. Atapour *et al.*, “Corrosion behavior of Ti-6Al-4V with different thermomechanical treatments and microstructures”, *Corrosion*, vol. 66, no. 6, 2010. doi:10.5006/1.3452400

[18] T. Ni and J. Dong, “Creep behaviors and mechanisms of INCONEL718 and allvac718plus”, *Materials Science and Engineering: A*, vol. 700, p. 406–415, 2017. doi:10.1016/j.msea.2017.06.032

[19] J. Hald, “Microstructure and long-term creep properties of 9–12% Cr Steels”, *International Journal of Pressure Vessels and Piping*, vol. 85, no. 1–2, p. 30–37, 2008. doi:10.1016/j.ijpvp.2007.06.010

[20] R. J. Smith, G. J. Lewi, and D. H. Yates, “Development and application of nickel alloys in aerospace engineering”, *Aircraft Engineering and Aerospace Technology*, vol. 73, no. 2, p. 138–147, 2001. doi:10.1108/00022660110694995

[21] J. F. Radavich, “Long time stability of a wrought alloy 718 disk”, *Superalloys 718 Metallurgy and Applications (1989)*, 1989. doi:10.7449/1989/superalloys_1989_257_268

[22] J. J. Schirra, R. H. Caless, and R. W. Hatala, “The effect of Laves phase on the mechanical properties of wrought and cast + hip inconel 718”, *Superalloys 718, 625 and Various Derivatives (1991)*, 1991. doi:10.7449/1991/superalloys_1991_375_388

[23] M. Sundararaman, L. Kumar, G. E. Prasad, P. Mukhopadhyay and S. Banerjee, “Precipitation of an intermetallic phase with Pt_2Mo-type structure in alloy 625”, *Metallurgical and Materials Transactions A,* vol. 30A, pp. 41–52, 1999.

[24] S. Hans, J.-M. Ruppert, and A. Mitchell, “Spot segregation in alloy INCO 718”, *Metallurgical and Materials Transactions A*, vol. 54, no. 8, pp. 3199–3210, 2023. doi:10.1007/s11661-023-07088-8

[25] R. F. Decker, “The evolution of wrought age-hardenable superalloys”, *Journal of Materials*, vol. 58, no. 9, p. 32–36, 2006. doi:10.1007/s11837-006-0079-8

[26] B. K. Damkroger *et al.*, “The influence of var processes and parameters on white spot formation in alloy 718”, *Superalloys 718, 625, 706 and Various Derivatives (1994)*, 1994. doi:10.7449/1994/superalloys_1994_125_135

[27] T. Seshacharyulu, S. C. Medeiros, W. G. Frazier, and Y. V. R. K. Prasad, “Microstructural mechanisms during hot working of commercial grade Ti–6Al–4V with lamellar starting structure”, *Materials Science and Engineering: A*, vol. 325, no. 1–2, p. 112–125, 2002. doi:10.1016/s0921-5093(01)01448-4

[28] M. Kulakov, S. Rahimi, and S. L. Semiatin, “Effect of deformation heating on microstructure evolution during hot forging of Ti-6Al-4V”, *Metallurgical and Materials Transactions A,* vol. 53, no. 2, p. 407–419, 2021. doi:10.1007/s11661-021-06493-1

[29] L. Li, J. Luo, J. J. Yan, and M. Q. Li, “Dynamic globularization and restoration mechanism of Ti–5Al–2Sn–2Zr–4Mo–4Cr alloy during isothermal compression”, *Journal of Alloys and Compounds*, vol. 622, p. 174–183, 2015. doi:10.1016/j.jallcom.2014.10.043

[30] M. O. Bodunrin, L. H. Chown, J. W. van der Merwe, and K. K. Alaneme, “Microstructural evolution during hot forming of Ti-6Al-4V alloy with complex initial microstructure”, *The International Journal of Advanced Manufacturing Technology,* vol. 104, no. 5–8, p. 3017–3026, 2019. doi:10.1007/s00170-019-04162-7

[31] G. Shen and D. Furrer, “Manufacturing of aerospace forgings”, *Journal of Materials Processing Technology,* vol. 98, no. 2, p. 189–195, 2000. doi:10.1016/s0924-0136(99)00198-3

[32] T. Seshacharyulu, S. C. Medeiros, W. G. Frazier, and Y. V. R. K. Prasad, “Hot working of commercial Ti–6Al–4V with an equiaxed α–β microstructure: Materials modeling considerations”,

Materials Science and Engineering: A, vol. 284, no. 1–2, p. 184–194, 2000. doi:10.1016/s0921-5093(00)00741-3

[33] S. C. Medeiros, Y. V. R. K. Prasad, W. G. Frazier, and R. Srinivasan, "Microstructural modeling of metadynamic recrystallization in hot working of in 718 superalloy", *Materials Science and Engineering: A*, vol. 293, no. 1–2, p. 198–207, 2000. doi:10.1016/s0921-5093(00)01053-4

[34] S. C. Krishna *et al.*, "Closed die hammer forging of Inconel 718", *Journal of Metallurgy*, vol. 2014, p. 1–7, 2014. doi:10.1155/2014/972917

[35] F. J. Zanner *et al.*, "Vacuum arc remelting of alloy 718", *Superalloys 718 Metallurgy and Applications (1989)*, 1989. doi:10.7449/1989/superalloys_1989_17_32

[36] B. K. Damkroger *et al.*, "The influence of var processes and parameters on white spot formation in alloy 718", *Superalloys 718, 625, 706 and Various Derivatives (1994)*, 1994. doi:10.7449/1994/superalloys_1994_125_135

[37] C. Malara and J. Radavich, "Alloy 718 large ingots studies", *Superalloys 718, 625, 706 and Various Derivatives (2005)*, 2005. doi:10.7449/2005/superalloys_2005_25_33

[38] C. Wang et al., "Interaction between γ′ precipitate distribution and microstructure homogeneity during hot deformation in a ni-based superalloy," Journal of Iron and Steel Research International, vol. 30, no. 11, pp. 2301–2317, Jul. 2023. doi:10.1007/s42243-023-01019-y

Appendix A: Standards Used in this Report

ASTM E112-13: Standard Test Methods for Determining Average Grain Size